JOURNAL OF GUIDANCE, CONTROL, AND DYNAMICS
Vol. 32, No. 2, March–April 2009

Motion and Parameter Estimation of Space Objects Using Laser-Vision Data

Farhad Aghili* and Kourosh Parsa†
Canadian Space Agency, Saint-Hubert, Quebec J3Y 8Y9, Canada

DOI: 10.2514/1.37129

A computationally efficient noise-adaptive Kalman filter is presented for the motion estimation and prediction of a free-falling tumbling satellite (target). The filter receives only noisy pose measurements from a laser-vision system aboard another satellite (chaser) at a close distance in a neighboring orbit. The filter estimates the full states, all the inertia parameters of the target satellite, and the covariance of the measurement noise. A comprehensive dynamics model that includes aspects of orbital mechanics is incorporated for accurate estimation. The discrete-time model, which involves a state-transition matrix and the covariance of process noise, is derived in closed form, thus rendering the filter suitable for real-time implementation. The statistical characteristics of the measurement noise is formulated by a state-dependent covariance matrix. This model allows additive quaternion noise, while preserving the unit-norm property of the quaternion. The convergence properties of the developed filter is demonstrated by simulation and experimental results. These results also demonstrate that the filter can continuously produce accurate estimates of pose even when the vision system is occluded for tens of seconds.

Nomenclature

$\underline{\boldsymbol{a}}$	=	$[\,\boldsymbol{a}^T \quad 0\,]^T \in \mathbb{R}^4$
$E(\cdot)$	=	expected value of $(\cdot)$
$\boldsymbol{e}_k$	=	discrete estimation error
$\boldsymbol{H}_k$	=	sensitivity matrix
I_{xx}, I_{yy}, I_{zz}	=	moments of inertia of the target satellite
$\boldsymbol{K}_k$	=	Kalman-filter gain matrix
$\boldsymbol{M}$ and $\boldsymbol{N}$	=	Jacobians of $\boldsymbol{\psi}(\boldsymbol{\omega}, \boldsymbol{p})$ with regard to $\boldsymbol{\omega}$ and $\boldsymbol{p}$
n	=	angular velocity of the orbit
$\boldsymbol{P}_k$	=	discrete covariance matrix of estimated states
$\boldsymbol{p}$, $\bar{\boldsymbol{p}}$, $\hat{\boldsymbol{p}}$	=	actual, nominal, and estimated inertia ratios of the target satellite
$\boldsymbol{Q}_{r_k}, \boldsymbol{Q}_{t_k}$	=	discrete covariance of the rotational and translational systems
$\boldsymbol{Q}_{\theta k}$	=	discrete covariance of the target parameters $\boldsymbol{\theta}$
$\boldsymbol{q}$, $\bar{\boldsymbol{q}}$, $\hat{\boldsymbol{q}}$	=	actual, nominal, and estimated quaternions representing the orientation of $\{\mathcal{B}\}$ with regard to $\{\mathcal{A}\}$
$\boldsymbol{q}^*$	=	conjugate of quaternion $\boldsymbol{q}$
R_e	=	radius of the circular orbit
$\boldsymbol{R}(\cdot)$	=	rotation matrix corresponding to quaternion $(\cdot)$
$\boldsymbol{r}$, $\hat{\boldsymbol{r}}$	=	actual and estimated position vectors connecting two centers of mass expressed in $\{\mathcal{A}\}$

Farhad Aghili is a federal Research Scientist at Canadian Space Agency (CSA), Saint-Hubert, Canada. He received a B.Sc. in mechanical engineering (1988) and a M.Sc. in biomedical engineering (1991) from Sharif University of Technology, Tehran, Iran, and a Ph.D. in mechanical engineering (1998) from McGill University, Montreal, Canada. During 1994–1997, he was a Research Engineer at MPB Technologies, Montreal. In January 1998, Dr. Aghili joined the CSA and worked on the International Space Station program. He has published more than 80 papers in journals and conference proceedings and is the author of 6 patents and patent applications in the United States and Canada. Dr. Aghili won the Best Paper Award at the 2007 ASME/IEEE International Conference on Mechatronic and Embedded Systems. He is a Member of the AIAA and a Senior Member of the Institute of Electrical and Electronics Engineers. His research interests combine multibody dynamics, robotic control, space robotics, vision systems, adaptive and robust control, and mechatronics systems.

Kourosh Parsa received B.S. and M.Sc. degrees in mechanical engineering from Sharif University of Technology, Tehran, Iran, in 1989 and 1993, respectively, and a Ph.D. degree from McGill University, Montreal, Canada, in 2003. Before starting his doctoral studies, he worked for about four years on automated material handling systems at an automobile manufacturing company in Tehran, where he helped design the very first industrial automated guided vehicle in Iran from the ground up. He worked as a Postdoctoral Fellow at the University of California, Davis from 2003 to 2004 on a suboptimal design of an all-accelerometer sensor array to be integrated in a Global-Positioning-System-assisted navigation system. From 2004 to 2007, he was a Visiting Fellow at the Space Technologies division of the Canadian Space Agency, where he worked on the robotic servicing of satellites on orbit. Since then, he has joined ESAB Cutting Systems. His interests include dynamics modeling and control of structurally flexible multibody systems, space robotics, analytical dynamics, and sensor design. Dr. Parsa is a registered Professional Engineer in the Province of Ontario, Canada.

Presented as Paper 7317 at the AIAA Guidance, Navigation and Control Conference and Exhibit, Honolulu, HI, 18–21 August 2008; received 13 February 2008; revision received 23 October 2008; accepted for publication 23 October 2008.

*Research Scientist, Space Technologies, 6767 Route de l'Aéroport.
†Visiting Fellow, Space Technologies; currently ESAB Welding & Cutting Products, Florence, SC.

$\boldsymbol{r}_c, \hat{\boldsymbol{r}}_c, \check{\boldsymbol{r}}_c$ = actual, estimated, and measured positions of the target expressed in $\{\mathcal{A}\}$
$\boldsymbol{r}_e$ = position vector connecting the Earth center to chaser's center of mass expressed in $\{\mathcal{A}\}$
$\boldsymbol{S}_k$ = discrete covariance of measurement noise
T_Δ = sampling time
$\boldsymbol{v}_k$ = additive measurement noise
$\text{vec}(\boldsymbol{q})$ = vector part of quaternion $\boldsymbol{q}$
$\boldsymbol{x}_r, \boldsymbol{x}_t$ = state of the rotational and the translational systems
$\boldsymbol{z}_k$ = vector of discrete observation
$\epsilon_f, \boldsymbol{\epsilon}_\tau$ = force and torque disturbances per unit inertia and mass on the target
$\boldsymbol{\epsilon}_\mu, \boldsymbol{\epsilon}_\varphi$ = errors associated with the quaternion $\boldsymbol{\mu}$ and the Euler angles $\boldsymbol{\varphi}$
$\boldsymbol{\eta}, \bar{\boldsymbol{\eta}}, \hat{\boldsymbol{\eta}}$ = actual, nominal, and estimated quaternions representing the orientation of $\{\mathcal{C}\}$ with regard to $\{\mathcal{B}\}$
$\boldsymbol{\theta}$ = vector parameterizing the center-of-mass position and the principal axis orientation of the target satellite
λ_i = ith eigenvalue of matrix $\boldsymbol{M}$
$\boldsymbol{\mu}, \hat{\boldsymbol{\mu}}, \check{\boldsymbol{\mu}}$ = actual, estimated, and measured quaternions representing the orientation of $\{\mathcal{C}\}$ with regard to $\{\mathcal{A}\}$
μ_e = gravitational parameter of Earth
$\boldsymbol{\rho}_c$ = location of the chaser satellite's center of mass expressed in $\{\mathcal{A}\}$
$\boldsymbol{\rho}_t, \hat{\boldsymbol{\rho}}_t$ = actual and estimated locations of the target satellite's center of mass expressed in $\{\mathcal{B}\}$
$\boldsymbol{\Sigma}_{r_k}, \boldsymbol{\Sigma}_{\mu_k}$ = covariances of the uncorrelated measurement noise associated with position and attitude
$\boldsymbol{\Phi}_r, \boldsymbol{\Phi}_t$ = state-transition matrices of the rotational and the translational systems
$\boldsymbol{\varphi}$ = vector containing Euler angles α, β, and γ
$\boldsymbol{\chi}, \hat{\boldsymbol{\chi}}$ = actual and estimated state vectors
${}^a\boldsymbol{\chi}$ = redundant state vector containing full quaternions
$\boldsymbol{\psi}(\boldsymbol{\omega}, \boldsymbol{p})$ = nonlinear vector of the Euler equation
$\boldsymbol{\omega}, \bar{\boldsymbol{\omega}}, \hat{\boldsymbol{\omega}}$ = actual, nominal, and estimated angular velocities of the target satellite expressed in $\{\mathcal{B}\}$
$\boldsymbol{\omega}_n$ = angular velocity of the chaser satellite expressed in $\{\mathcal{B}\}$
$\boldsymbol{\omega}_{\text{rel}}$ = relative angular velocity of the target satellite with regard to the chaser expressed in $\{\mathcal{B}\}$
ϖ = norm of the nominal angular velocity $\bar{\boldsymbol{\omega}}$
$\mathbf{1}_n$ = $n \times n$ identity matrix
$\lceil \cdot \rceil$ = matrix form of the cross product
$\otimes, \circledast$ = quaternion products

I. Introduction

THERE has been growing worldwide interest in using space robotic systems for the on-orbit servicing of spacecraft [1–6]. In such missions, the accurate estimation of the motion of a free-falling target spacecraft is essential for its capture with a robotic arm. Different perception systems are available for the estimation of the pose (position and orientation) of moving objects. Among these systems, an active vision system such as the Laser Camera System (LCS) is preferable for its robustness in face of the harsh lighting conditions of space [7]. As successfully verified during the STS-105 space mission, the 3-D imaging technology used in the LCS can indeed operate in the space environment.

The use of laser range data has also been proposed for the motion estimation of free-floating[‡] space objects [8,9]. All vision systems, however, provide discrete and noisy pose data at relatively low rate, typically 1 Hz, and the capture of a free-falling object is a difficult robotic task that requires accurate real-time pose estimation. Moreover, the robotic capture of (or docking to) a space object requires a predictable trajectory for two reasons:

1) The robot motion must be planned to intercept the object at a rendezvous point [10–13].

2) In the case that vision data are not available (e.g., visual occlusion), the pose can still be predicted from the model.

In essence, the pose prediction requires accurate estimation of the system states and unknown parameters.

Taking advantage of the simple dynamics of a free-floating object, researchers have employed different observers to track and predict the motion of a target satellite [8,9,14–17]. In some circumstances (e.g., when there are occlusions), no observation data are available. Therefore, long-term prediction of the motion of the object is needed for planning operations such as the autonomous grasping of targets [9,14]. Motivated by the robotic servicing mission for the Hubble Space Telescope, Thienel and Sanner [16] developed a nonlinear algorithm to estimate the rotation rates for a noncooperative target vehicle. Although the nonlinear estimator is suitably implemented for the quaternion-based attitude kinematics, it does not take the properties of the sensor and process noises into account. Kim et al. [15] designed an extended Kalman filter (KF) for the estimation of the spacecraft relative pose in formation-flying applications. The filter uses line-of-sight observations coupled with gyro measurements from each spacecraft and does not incorporate the spacecraft attitude dynamics.

This paper proposes the design of an adaptive KF that uses the LCS data for the effective estimation and prediction of the relative pose of two spacecraft in nearby orbits. It is known that the applicability of the Kalman filtering technique rests on the accuracy of the measurement-noise models, and the accuracy of the LCS measured pose usually depends upon the range and geometry of the object. The larger the range, the less accurate the measured distance, and the more symmetrical the object (with a sphere being the most symmetrical), the less accurate the orientation measurement.

Because the filter is *noise-adaptive*, it can tune itself by identifying the covariance matrix of the measurement noise. Moreover, the adaptive KF estimates not only the full states of the system but also all inertial parameters of the space object, including the ratios of the object moments of inertia, the location of its center of mass (c.m.), and the orientation of its principal axes. That makes the trajectory of the space object predictable.

The full model of the rotational and translational motions, including aspects of *orbital mechanics*, are incorporated for accurate estimation. In addition, the state variables are defined so that most of the parameters appear in the observation matrix rather than the system dynamics. This leads to a simple discrete-time model requiring minimum computational burden. Furthermore, taking advantage of the structure of the model, we derive computationally efficient expressions for the system state-transition matrix and the covariance of the process noise; both expressions are necessary for the KF. Notably, the conventional solution to the state-transition matrix and discrete-time process noise, which is based on the van Loan method [18], involves computing the exponential of a large matrix,[§] a procedure beyond the computational power of many spacecraft onboard computers.

The kinematic properties of the unit-norm quaternions, used to represent the relative orientation of the target satellite, are employed to derive the associated measurement-noise covariance. The new model allows *additive* quaternion noise while preserving the unit-norm property of the quaternion. Next, an adaptive variant of the extended KF is used to estimate both the states and the covariance matrix of the measurement noise. This allows autonomous tuning of the filter as the noise characteristics of the vision system change. Finally, simulation and experiential results are reported that demonstrate the convergence property of the adaptive KF. These results are followed by other experimental results demonstrating the

[‡]By definition, a *free-falling* object is acted upon only by a gravitational force, whereas a *free-floating* object drifts in space with no external force whatsoever. As such, a free-floating object moves at a constant velocity with respect to an inertial frame.

[§]When the inertial parameters are to be estimated as well, the van Loan method requires computing the exponential function of an 18×18 and a 12×12 matrix.

performance of the filter in pose estimation when the vision system is occluded.

II. State Equations

Figure 1 illustrates the chaser and the target satellites as rigid bodies moving in nearby orbits. Coordinate frames $\{\mathcal{A}\}$ and $\{\mathcal{B}\}$ are attached to the chaser and the target, respectively. The origin of $\{\mathcal{B}\}$ is located at the target c.m. and that of $\{\mathcal{A}\}$ is at position $\boldsymbol{\rho}_c$ from the c.m. of the chaser. The axes of $\{\mathcal{B}\}$ are oriented to be parallel to the principal axes of the target satellite, and $\{\mathcal{A}\}$ is orientated so that its x axis is parallel to a line connecting the Earth's center to the chaser c.m. and pointing outward, and its y axis lies on the orbital plane (see Fig. 1). Coordinate frame $\{\mathcal{C}\}$ is fixed to the target at its point of reference located at $\boldsymbol{\rho}_t$ from the origin of $\{\mathcal{B}\}$. It is the pose of $\{\mathcal{C}\}$ that is measured by the laser camera. We further assume that the target satellite tumbles with angular velocity $\boldsymbol{\omega}$. Also notice that the coordinate frame $\{\mathcal{A}\}$ is not inertial; rather, it moves with the chaser satellite. In the following, vectors $\boldsymbol{\rho}_t$ and $\boldsymbol{\omega}$ are expressed in $\{\mathcal{B}\}$, and vector $\boldsymbol{\rho}_c$ is expressed in $\{\mathcal{A}\}$.

Here, we choose to express the target orientation in the body-attached frames coincident with its principal axes (i.e., $\{\mathcal{B}\}$), and the translational motion variables are expressed in the body-attached frame of the chaser (i.e., $\{\mathcal{A}\}$). The advantages of such a mixed coordinate selection are twofold: First, the inertia matrix becomes diagonal and will be independent of the target orientation, thus resulting in a simple attitude model. Second, choosing to express the relative translational motion dynamics in $\{\mathcal{A}\}$ leads to decoupled translational and rotational dynamics that greatly contribute to the simplification of the mathematical model; note that because $\{\mathcal{B}\}$ is a rotating frame, the translational acceleration seen from this frame depends on both the relative angular velocity and relative acceleration. In the following, subscripts r and t denote quantities associated with the rotational and translational dynamics of the system, respectively.

The orientation of $\{\mathcal{B}\}$ with respect to $\{\mathcal{A}\}$ is represented by the unit quaternion $\boldsymbol{q} = [\,\boldsymbol{q}_v^T \quad q_0\,]^T$, where subscripts v and 0 denote the vector and scalar parts of the quaternion, respectively. By definition, $\boldsymbol{q}_v = \boldsymbol{e}\sin\frac{\phi}{2}$ and $q_0 = \cos\frac{\phi}{2}$, where ϕ is the rotation angle, and $\boldsymbol{e}$ is the unit vector along the axis of rotation.

Next, we review some basic definitions and properties of quaternions used in the rest of the paper. Consider quaternions $\boldsymbol{q}_1, \boldsymbol{q}_2$, and $\boldsymbol{q}_3$ and their corresponding rotation matrices $\boldsymbol{R}_1$, $\boldsymbol{R}_2$, and $\boldsymbol{R}_3$, respectively. Operators $\otimes$ and $\circledast$ are defined as

$$
\begin{aligned}
[\boldsymbol{a}\otimes] &\triangleq \begin{bmatrix} -\lceil \boldsymbol{a}_v \rceil + a_o 1_3 & \boldsymbol{a}_v \\ -\boldsymbol{a}_v^T & a_o \end{bmatrix} \\
[\boldsymbol{a}\circledast] &\triangleq \begin{bmatrix} \lceil \boldsymbol{a}_v \rceil + a_o 1_3 & \boldsymbol{a}_v \\ -\boldsymbol{a}_v^T & a_o \end{bmatrix}, \quad \text{with} \quad \boldsymbol{a} \triangleq \begin{bmatrix} \boldsymbol{a}_v \\ a_0 \end{bmatrix}
\end{aligned}
\tag{1}
$$

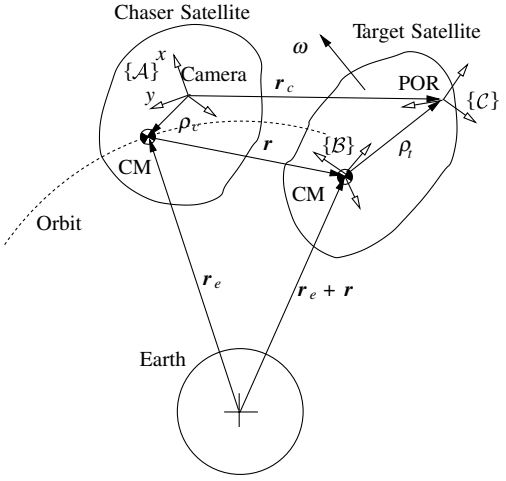

Fig. 1 Body diagram of chaser and target satellites moving in neighboring orbits (POR denotes the point of reference).

where $\lceil \boldsymbol{a}_v \rceil$ is the cross-product matrix of $\boldsymbol{a}_v$ (i.e., for all $\boldsymbol{b} \in \mathbb{R}^3$, where $\lceil \boldsymbol{a}_v \rceil \boldsymbol{b} = \boldsymbol{a}_v \times \boldsymbol{b}$). Then

$$
\boldsymbol{q}_3 = \boldsymbol{q}_2 \otimes \boldsymbol{q}_1 \equiv \boldsymbol{q}_1 \circledast \boldsymbol{q}_2 \tag{2}
$$

corresponds to product $\boldsymbol{R}_3 = \boldsymbol{R}_1 \boldsymbol{R}_2$. This simple composition rule is one major reason for choosing quaternions for orientation representation.

The conjugate quaternion $\boldsymbol{q}^*$ ($q_o^* = q_o$ and $\boldsymbol{q}_v^* = -\boldsymbol{q}_v$) of $\boldsymbol{q}$ is defined such that

$$
\boldsymbol{q}^* \otimes \boldsymbol{q} = \boldsymbol{q} \otimes \boldsymbol{q}^* = [\,0 \quad 0 \quad 0 \quad 1\,]^T
$$

Moreover, both $\otimes$ and $\circledast$ operations have associative properties; hence, $\boldsymbol{q}_1 \otimes \boldsymbol{q}_2 \otimes \boldsymbol{q}_3$ and $\boldsymbol{q}_1 \circledast \boldsymbol{q}_2 \circledast \boldsymbol{q}_3$ are unambiguous.

In the rest of this paper, the underlined form of any vector $\boldsymbol{a} \in \mathbb{R}^3$ denotes the representation of that vector in $\mathbb{R}^4$, (e.g., $\underline{\boldsymbol{a}}^T \triangleq [\,\boldsymbol{a}^T \quad 0\,]$). Representing the orientation of the target satellite with respect to the chaser satellite with quaternion $\boldsymbol{q}$, we can express the relation between the time derivative of $\boldsymbol{q}$ and the relative angular velocity $\boldsymbol{\omega}_{\text{rel}}$ as

$$
\dot{\boldsymbol{q}} = \tfrac{1}{2}\underline{\boldsymbol{\omega}}_{\text{rel}} \otimes \boldsymbol{q} \tag{3}
$$

where $\boldsymbol{\omega}_{\text{rel}} = \boldsymbol{\omega} - \boldsymbol{\omega}_n$, and $\boldsymbol{\omega}_n$ is the angular velocity of the chaser satellite expressed in frame $\{\mathcal{B}\}$. Moreover, it is assumed that the attitude-control system of the chaser satellite makes it rotate with the angular velocity of the reference orbit. Furthermore, denoting the angular velocity of the reference orbit expressed in $\{\mathcal{A}\}$ with

$$
\boldsymbol{n} \equiv [\,0 \quad 0 \quad n\,]^T \tag{4}
$$

one can relate $\boldsymbol{n}$ and $\boldsymbol{\omega}_n$ using the following quaternion transformation [19]:

$$
\underline{\boldsymbol{\omega}}_n = \boldsymbol{q} \otimes \underline{\boldsymbol{n}} \otimes \boldsymbol{q}^* \tag{5}
$$

Substituting Eq. (5) into Eq. (3) and using the properties of the quaternion products, we arrive at

$$
\dot{\boldsymbol{q}} = \tfrac{1}{2}\underline{\boldsymbol{\omega}} \otimes \boldsymbol{q} - \tfrac{1}{2}(\boldsymbol{q} \otimes \underline{\boldsymbol{n}}) \otimes (\boldsymbol{q}^* \otimes \boldsymbol{q}) = \tfrac{1}{2}(\underline{\boldsymbol{\omega}} \otimes -\underline{\boldsymbol{n}}\circledast)\boldsymbol{q} \tag{6}
$$

The quaternion associated with the rotation from the nominal orientation $\bar{\boldsymbol{q}}$ to the actual orientation $\boldsymbol{q}$ can be obtained from Eq. (2) as

$$
\delta\boldsymbol{q} = \boldsymbol{q} \otimes \bar{\boldsymbol{q}}^* \tag{7}
$$

Adopting a technique similar to that used by other authors [20,21], one can then linearize the time derivative of the preceding equation about the estimated states $\bar{\boldsymbol{q}}$ and $\bar{\boldsymbol{\omega}}$, as shown in Appendix A, to obtain

$$
\frac{d}{dt}\delta\boldsymbol{q}_v \approx -\bar{\boldsymbol{\omega}} \times \delta\boldsymbol{q}_v + \frac{1}{2}\delta\boldsymbol{\omega}, \qquad \frac{d}{dt}\delta q_o \approx 0 \tag{8}
$$

The right-hand-side equation can be ignored because δq_o is not an independent variable and it has only variations of the second order [20]. It is interesting to note that the angular velocity of the chaser satellite does not affect the preceding linearized equation.

Denoting the principal moments of inertia of the target satellite with I_{xx}, I_{yy}, and I_{zz}, we define the inertia ratios:

$$
p_x = \frac{I_{yy} - I_{zz}}{I_{xx}}, \qquad p_y = \frac{I_{zz} - I_{xx}}{I_{yy}}, \qquad p_z = \frac{I_{xx} - I_{yy}}{I_{zz}}
$$

According to Euler's equation, the dynamics of the rotational motion of the target satellite can be expressed in terms of the new parameters as

$$
\dot{\boldsymbol{\omega}} = \boldsymbol{\psi}(\boldsymbol{\omega}) + \boldsymbol{J}(\boldsymbol{p})\boldsymbol{\epsilon}_\tau \tag{9}
$$

where

$$\boldsymbol{\psi}(\boldsymbol{\omega}) = \begin{bmatrix} p_x\omega_y\omega_z \\ p_y\omega_x\omega_z \\ p_z\omega_x\omega_y \end{bmatrix}, \qquad \boldsymbol{J}(\boldsymbol{p}) = \begin{bmatrix} 1 & 0 & 0 \\ 0 & \frac{1-p_y}{1+p_x} & 0 \\ 0 & 0 & \frac{1+p_z}{1-p_x} \end{bmatrix}$$

(see Appendix B for details). Linearizing Eq. (9) about $\bar{\boldsymbol{\omega}}$ and $\bar{\boldsymbol{p}}$ yields

$$\frac{d}{dt}\delta\boldsymbol{\omega} = \boldsymbol{M}(\bar{\boldsymbol{\omega}}, \bar{\boldsymbol{p}})\delta\boldsymbol{\omega} + \boldsymbol{N}(\bar{\boldsymbol{\omega}})\delta\boldsymbol{p} + \boldsymbol{J}(\bar{\boldsymbol{p}})\boldsymbol{\epsilon}_\tau \tag{10}$$

where $\boldsymbol{p}^T = [\, p_x \quad p_y \quad p_z \,]$,

$$\begin{aligned} \boldsymbol{M}(\boldsymbol{\omega}, \boldsymbol{p}) &= \frac{\partial \boldsymbol{\psi}}{\partial \boldsymbol{\omega}} = \begin{bmatrix} 0 & p_x\omega_z & p_x\omega_y \\ p_y\omega_z & 0 & p_y\omega_x \\ p_z\omega_y & p_z\omega_x & 0 \end{bmatrix} \\ \boldsymbol{N}(\boldsymbol{\omega}) &= \frac{\partial \boldsymbol{\psi}}{\partial \boldsymbol{p}} = \begin{bmatrix} \omega_y\omega_z & 0 & 0 \\ 0 & \omega_x\omega_z & 0 \\ 0 & 0 & \omega_x\omega_y \end{bmatrix} \end{aligned} \tag{11}$$

Let vector $\boldsymbol{x}_r^T = [\, \boldsymbol{q}_v^T \quad \boldsymbol{\omega}^T \quad \boldsymbol{p}^T \,]$ describe the part of the system states pertaining to rotational motion. Setting Eqs. (8) and (10) in the state-space form, we obtain

$$\frac{d}{dt}\delta\boldsymbol{x}_r = \begin{bmatrix} -\lceil\bar{\boldsymbol{\omega}}\rceil & \frac{1}{2}\mathbf{1}_3 & \mathbf{0}_{3\times3} \\ \mathbf{0}_{3\times3} & \boldsymbol{M}(\bar{\boldsymbol{\omega}}, \bar{\boldsymbol{p}}) & \boldsymbol{N}(\bar{\boldsymbol{\omega}}) \\ \mathbf{0}_{3\times3} & \mathbf{0}_{3\times3} & \mathbf{0}_{3\times3} \end{bmatrix}\delta\boldsymbol{x}_r + \begin{bmatrix} \mathbf{0}_{3\times3} \\ \boldsymbol{J}(\bar{\boldsymbol{p}}) \\ \mathbf{0}_{3\times3} \end{bmatrix}\boldsymbol{\epsilon}_\tau \tag{12}$$

In addition to the inertia of the target satellite, the location of its c.m. and the orientation of the principal axes $\boldsymbol{\eta}_v$ are uncertain. Denoting the additional unknown parameters pertaining to the position and orientation of $\{\mathcal{C}\}$ with vector $\boldsymbol{\theta}^T = [\, \boldsymbol{\rho}_t^T \quad \boldsymbol{\eta}_v^T \,]$, we have

$$\dot{\boldsymbol{\theta}} = \mathbf{0}_{6\times1} \tag{13}$$

The evolution of the relative position of the two satellites can be described by the Euler–Hill model in *orbital mechanics*. Let the chaser move on a circular orbit with radius R_e, thus the carrier has an angular rate n. Further, assume that vector $\boldsymbol{r}$ denotes the relative position of the c.m. of the two satellites expressed in frame $\{\mathcal{A}\}$. The translational motion of the target can then be expressed as

$$\ddot{\boldsymbol{r}} = -2\boldsymbol{n}\times\dot{\boldsymbol{r}} - \boldsymbol{n}\times(\boldsymbol{n}\times\boldsymbol{r}) + \left(-\mu_e\frac{\boldsymbol{r}_e + \boldsymbol{r}}{\|\boldsymbol{r}_e + \boldsymbol{r}\|^3} + n^2\boldsymbol{r}_e\right) + \boldsymbol{\epsilon}_f \tag{14}$$

where μ_e is the gravitational parameter of the Earth, and $\boldsymbol{r}_e = [\, R_e \quad 0 \quad 0 \,]^T$ is a constant position vector expressed in frame $\{\mathcal{A}\}$ that connects the Earth's center to the chaser c.m.. Note that the constant position vector can be computed from the angular rate of the circular orbit by

$$\boldsymbol{r}_e = \begin{bmatrix} \sqrt[3]{\frac{\mu_e}{n^2}} & 0 & 0 \end{bmatrix}^T \tag{15}$$

Denoting the states of the translational motion with $\boldsymbol{x}_t^T = [\, \boldsymbol{r}^T \quad \dot{\boldsymbol{r}}^T \,]$, the linearized translational dynamics about $\boldsymbol{r} = \mathbf{0}_{3\times1}$ is given by

$$\frac{d}{dt}\delta\boldsymbol{x}_t = \begin{bmatrix} \mathbf{0}_{3\times3} & \mathbf{1}_3 \\ \boldsymbol{K}(n) & -2\lceil\boldsymbol{n}\rceil \end{bmatrix}\delta\boldsymbol{x}_t + \begin{bmatrix} \mathbf{0}_{3\times3} \\ \mathbf{1}_3 \end{bmatrix}\boldsymbol{\epsilon}_f \tag{16}$$

with

$$\boldsymbol{K}(n) = \begin{bmatrix} 3n^2 & 0 & 0 \\ 0 & 0 & 0 \\ 0 & 0 & -n^2 \end{bmatrix}$$

which are known as the Euler–Hill equations [22] or the Clohessy–Wiltshire equations [23].

III. Discrete Model

A. State-Transition Matrix

To take the composition rules of quaternions into account, the state vector to be estimated by the KF is defined as

$$\boldsymbol{\chi} \triangleq [\, \delta\boldsymbol{q}_v^T \quad \boldsymbol{\omega}^T \quad \boldsymbol{p}^T \quad \boldsymbol{r}^T \quad \dot{\boldsymbol{r}}^T \quad \boldsymbol{\rho}_t^T \quad \delta\boldsymbol{\eta}_v^T \,]^T \in \mathbb{R}^{21} \tag{17}$$

where $\delta\boldsymbol{\eta}$, defined as

$$\delta\boldsymbol{\eta} \triangleq \bar{\boldsymbol{\eta}}^* \otimes \boldsymbol{\eta} \tag{18}$$

is the deviation of quaternion $\boldsymbol{\eta}$ from its nominal value $\bar{\boldsymbol{\eta}}$, defined analogous to Eq. (7). From the linearized continuous-time systems (12), (13), and (16), we can then derive the linearized discrete-time system representing the state vector $\boldsymbol{\chi}_k$ as

$$\boldsymbol{\chi}_{k+1} = \boldsymbol{\Phi}_k\boldsymbol{\chi}_k + \boldsymbol{\epsilon}_k \tag{19}$$

where $\boldsymbol{\Phi}_k = \boldsymbol{\Phi}(t_k; T_\Delta)$ is the state-transition matrix of the entire system, $T_\Delta = t_{k+1} - t_k$ is the sampling time, and $\boldsymbol{\epsilon}_k$ is the equivalent discrete-time process noise. Because dynamics models pertaining to systems (12), (13), and (16), are decoupled from each other, the state-transition matrix takes a block diagonal form:

$$\boldsymbol{\Phi} = \operatorname{diag}(\boldsymbol{\Phi}_r, \boldsymbol{\Phi}_t, \mathbf{1}_6)$$

where $\boldsymbol{\Phi}_r$ and $\boldsymbol{\Phi}_t$ are the state-transition matrices associated with the rotational and translational systems, respectively. The closed-form relation of $\boldsymbol{\Phi}_r$ and $\boldsymbol{\Phi}_t$ are derived subsequently.

1. Rotational Motion

Assuming $0 \le t \le T_\Delta$, we can write the state-transition matrix $\boldsymbol{\Phi}_r$, pertaining to Eq. (12), as

$$\boldsymbol{\Phi}_r(t) = \begin{bmatrix} \boldsymbol{\Phi}_{r_{11}}(t) & \boldsymbol{\Phi}_{r_{12}}(t) & \boldsymbol{\Phi}_{r_{13}}(t) \\ \mathbf{0}_{3\times3} & \boldsymbol{\Phi}_{r_{22}}(t) & \boldsymbol{\Phi}_{r_{23}}(t) \\ \mathbf{0}_{3\times3} & \mathbf{0}_{3\times3} & \mathbf{1}_3 \end{bmatrix}$$

where

$$\boldsymbol{\Phi}_{r_{11}}(t) = e^{-\lceil\bar{\boldsymbol{\omega}}_k\rceil t} = \mathbf{1}_3 - \frac{\sin\varpi_k t}{\varpi_k}\lceil\bar{\boldsymbol{\omega}}_k\rceil + \frac{1-\cos\varpi_k t}{\varpi_k^2}\lceil\bar{\boldsymbol{\omega}}_k\rceil^2 \tag{20a}$$

$$\boldsymbol{\Phi}_{r_{12}}(t) = \frac{1}{2}\sum_{i,j,k}^{3}\gamma_{ij}\phi'_{jk}\lceil\bar{\boldsymbol{\omega}}_k\rceil^{k-1}\boldsymbol{M}^{i-1} \tag{20b}$$

$$\boldsymbol{\Phi}_{r_{13}}(t) = \sum_{i,j}^{3}\gamma_{ij}\lambda_j^{-1}(e^{\lambda_j t} - 1)\boldsymbol{M}^{i-1}\boldsymbol{N} \tag{20c}$$

$$\boldsymbol{\Phi}_{r_{22}}(t) = e^{\boldsymbol{M}(\bar{\boldsymbol{\omega}}_k)t} = \sum_{i,j}^{3}\gamma_{ij}e^{\lambda_j t}\boldsymbol{M}^{i-1} \tag{20d}$$

$$\boldsymbol{\Phi}_{r_{23}}(t) = \frac{1}{2}\sum_{i,j,k}^{3}\gamma_{ij}\phi_{jk}\lceil\bar{\boldsymbol{\omega}}_k\rceil^{k-1}\boldsymbol{M}^{i-1}\boldsymbol{N} \tag{20e}$$

In the preceding, γ_{ij} can be constructed from the eigenvalues as described in Appendix C, scalar functions $\phi'_{kj}(t)$ and

$$\phi_{kj}(t) = \int_0^t \phi'_{kj}(\tau)\mathrm{d}\tau$$

are given in explicit form in Appendix D, and $\varpi_k = \|\bar{\boldsymbol{\omega}}_k\|$.

2. Translational Motion

The 6×6 state-transition matrix for the translational system (16) can be derived as

$$\boldsymbol{\Phi}_t(t) = \begin{bmatrix} 4-3\cos nt & 0 & 0 & \frac{1}{n}\sin nt & \frac{2}{n}(1-\cos nt) & 0 \\ 6(\sin nt - nt) & 1 & 0 & 4(\cos nt - 1) & \frac{4}{n}\sin nt - 3t & 0 \\ 0 & 0 & \cos nt & 0 & 0 & \frac{1}{n}\sin nt \\ 3n\sin nt & 0 & 0 & \cos nt & 2\sin nt & 0 \\ 6n(\cos nt - 1) & 0 & 0 & -2\sin nt & 4\cos nt - 3 & 0 \\ 0 & 0 & -n\sin nt & 0 & 0 & \cos nt \end{bmatrix}, \qquad 0 \le t \le T_\Delta \tag{21}$$

Apparently, the elements of matrix $\boldsymbol{\Phi}_t$ are trigonometric functions of dimensionless variable $a \triangleq nt$, which can be treated as the rotation angle of the chaser at time t. Thus, writing the Taylor expansion of Eq. (21) about $a = 0$ (for $0 \le t \le T_\Delta$), we obtain

$$\boldsymbol{\Phi}_t(t) = \begin{bmatrix} \mathbf{1}_3 & \boldsymbol{\Phi}_{t_{12}}(t) \\ \mathbf{0}_{3\times 3} & \boldsymbol{\Phi}_{t_{22}}(t) \end{bmatrix} + \mathcal{O}(a^2) \tag{22}$$

where

$$\boldsymbol{\Phi}_{t_{12}}(t) = \begin{bmatrix} t & nt^2 & 0 \\ 0 & t & 0 \\ 0 & 0 & t \end{bmatrix}, \qquad \boldsymbol{\Phi}_{t_{22}}(t) = \mathbf{1}_3 - 2\lceil \boldsymbol{n} \rceil t$$

Because the angular velocity of the reference orbit is a small variable, we can say that for $0 < t \le T_\Delta$, $nt \ll 1$.[¶] Thus, we can dramatically simplify the expression of the state-transition matrix (21) by eliminating the second- and higher-order terms of nt in Eq. (22). That is, $\boldsymbol{\Phi}_t$ can be effectively approximated by the first term on the right-hand side (RHS) of Eq. (22).

3. Parameters

Let $\boldsymbol{\theta}_k$ be the discrete-time form of the c.m. parameters, which are to be estimated by the KF. Because $\boldsymbol{\theta}_k$ is a constant vector, it seems quite natural to describe the dynamics associated with the parameters by $\boldsymbol{\theta}_{k+1} = \boldsymbol{\theta}_k$. However, it is known that if the vector $\boldsymbol{\theta}$ of unknown parameters is considered to be deterministic, then it cannot be identified via an extended Kalman filter [24]. This occurs because the filter becomes overconfident in the model in the absence of process noise, and it consequently does not incorporate the measurements in the estimation process. As such, $\boldsymbol{\theta}$ must be treated as a random constant vector as

$$\boldsymbol{\theta}_{k+1} = \boldsymbol{\theta}_k + \boldsymbol{\epsilon}_{\theta_k} \tag{23}$$

where $\boldsymbol{\epsilon}_{\theta_k}$ is a fictitious zero-mean Gaussian white-noise sequence with $\boldsymbol{Q}_{\theta_k} = E[\boldsymbol{\epsilon}_{\theta_k}\boldsymbol{\epsilon}_{\theta_k}^T]$. Typically, we can select $\boldsymbol{Q}_{\theta_k} = \sigma_\theta^2 \mathbf{1}_6$, whereby σ_θ is treated as one of the tuning parameters of the filter.

B. Covariance Matrix of Process Noise

In our model, the effects of flexible appendages such as solar panels, the gravity gradient, and the fuel sloshing are not considered because, in practice, it is usually sufficient to model them as process noise in the KF [8]. Presumably, the continuous process noise is with covariances

$$\boldsymbol{\Sigma}_\tau = E[\boldsymbol{\epsilon}_\tau \boldsymbol{\epsilon}_\tau^T] = \sigma_\tau^2 \mathbf{1}_3$$

and

$$\boldsymbol{\Sigma}_f = E[\boldsymbol{\epsilon}_f \boldsymbol{\epsilon}_f^T] = \sigma_f^2 \mathbf{1}_3$$

Let $\boldsymbol{Q}_k = \mathrm{diag}(\boldsymbol{Q}_{r_k}, \boldsymbol{Q}_{t_k}, \boldsymbol{Q}_{\theta_k})$ be the covariance matrix of the entire process noise, which will be used in the KF. Covariance $\boldsymbol{Q}_{r_k}$ can be calculated from

$$\boldsymbol{Q}_{r_k} = E[\boldsymbol{\epsilon}_{r_k}\boldsymbol{\epsilon}_{r_k}^T] = \int_{t_k}^{t_{k+1}} \boldsymbol{\Phi}_{r_k}(t)\boldsymbol{G}_{r_k}\boldsymbol{\Sigma}_\tau \boldsymbol{G}_{r_k}^T \boldsymbol{\Phi}_{r_k}^T(t)\mathrm{d}t \tag{24}$$

with $\boldsymbol{G}_{r_k}^T = [\mathbf{0}_{3\times 3}\ \boldsymbol{J}(p_k)\ \mathbf{0}_{3\times 3}]$, thus resulting in

$$\boldsymbol{Q}_{r_k} = \begin{bmatrix} \boldsymbol{Q}_{r_{k11}} & \boldsymbol{Q}_{r_{k12}} & \mathbf{0}_{3\times 3} \\ \boldsymbol{Q}_{r_{k12}}^T & \boldsymbol{Q}_{r_{k22}} & \mathbf{0}_{3\times 3} \\ \mathbf{0}_{3\times 3} & \mathbf{0}_{3\times 3} & \boldsymbol{Q}_{p_k} \end{bmatrix}$$

where

$$\boldsymbol{Q}_{r_{k11}} = \sigma_\tau^2 \int_{t_k}^{t_{k+1}} \boldsymbol{\Phi}_{r_{12}} \boldsymbol{J}_k^2 \boldsymbol{\Phi}_{r_{12}}^T \mathrm{d}t,$$

$$\boldsymbol{Q}_{r_{k12}} = \sigma_\tau^2 \int_{t_k}^{t_{k+1}} \boldsymbol{\Phi}_{r_{12}} \boldsymbol{J}_k^2 \boldsymbol{\Phi}_{r_{22}}^T \mathrm{d}t, \qquad \boldsymbol{Q}_{r_{k22}} = \sigma_\tau^2 \int_{t_k}^{t_{k+1}} \boldsymbol{\Phi}_{r22} \boldsymbol{J}_k^2 \boldsymbol{\Phi}_{r_{22}}^T \mathrm{d}t \tag{25}$$

$\boldsymbol{Q}_{p_k} = \sigma_p^2 \mathbf{1}_3$ is the covariance matrix of the fictitious noise associated with parameter $\boldsymbol{p}$, and σ_p can be treated as another tuning parameter of the filter [similar to Eq. (23)].

Analogous to Eq. (24), the discrete-time covariance matrix associated with the force disturbance can be calculated from the state-transition matrix (21) and from $\boldsymbol{G}_{t_k}^T = [\mathbf{0}_{3\times 3} \quad \mathbf{1}_3]$. Neglecting the third-order terms and higher of a, we arrive at

$$\boldsymbol{Q}_{t_k} = E[\boldsymbol{\epsilon}_{t_k} \quad \boldsymbol{\epsilon}_{t_k}^T] = \sigma_f^2 \begin{bmatrix} \boldsymbol{Q}_{t_{k11}} & \boldsymbol{Q}_{t_{k12}} \\ \boldsymbol{Q}_{t_{k12}}^T & \boldsymbol{Q}_{t_{k22}} \end{bmatrix} + \mathcal{O}(a^3)$$

where

$$\boldsymbol{Q}_{t_{k11}} = \begin{bmatrix} \frac{1}{3}T_\Delta^3 + \frac{2}{5}n^2T_\Delta^5 & \frac{1}{4}(n-n^2)T_\Delta^4 & 0 \\ \frac{1}{4}(n-n^2)T_\Delta^4 & \frac{1}{3}T_\Delta^3 - \frac{4}{15}n^2T_\Delta^5 & 0 \\ 0 & 0 & \frac{1}{3}T_\Delta^3 - \frac{1}{15}n^2T_\Delta^5 \end{bmatrix}$$

$$\boldsymbol{Q}_{t_{k12}} = \begin{bmatrix} \frac{1}{2}T_\Delta^2 + \frac{1}{3}n^2T_\Delta^4 & -\frac{1}{3}nT_\Delta^3 & 0 \\ \frac{2}{3}(n-n^2)T_\Delta^3 & \frac{1}{2}T_\Delta^2 - \frac{2}{3}n^2T_\Delta^4 & 0 \\ 0 & 0 & \frac{1}{2}T_\Delta^2 - \frac{1}{6}n^2T_\Delta^4 \end{bmatrix}$$

$$\boldsymbol{Q}_{t_{k22}} = \begin{bmatrix} T_\Delta + n^2T_\Delta^3 & 0 & 0 \\ 0 & T_\Delta & 0 \\ 0 & 0 & T_\Delta - \frac{1}{3}n^2T_\Delta^3 \end{bmatrix}$$

C. Observation Matrix

The vision system (namely, the LCS) measures both the orientation of $\{\mathcal{C}\}$ and the position vector $\boldsymbol{r}_c$ of its origin in the LCS frame. That is,

$$\text{measured pose} \equiv \begin{bmatrix} \boldsymbol{r}_c \\ \boldsymbol{\mu} \end{bmatrix}$$

where

$$\boldsymbol{\mu} \triangleq \boldsymbol{\eta} \otimes \boldsymbol{q} \tag{26}$$

represents the orientation of $\{\mathcal{C}\}$ with regard to $\{\mathcal{A}\}$. Apparently, we have

[¶]Typically, $n = 0.0012$ rad/s and $0 < t \le 20$ s. Thus, $nt \le 0.024 \ll 1$.

$$\boldsymbol{r}_c = \boldsymbol{r} + \boldsymbol{\rho}_c + \boldsymbol{R}(\boldsymbol{q})\boldsymbol{\rho}_t \tag{27}$$

where every vector except $\boldsymbol{\rho}_t$ is expressed in $\{\mathcal{A}\}$, and $\boldsymbol{R}(\boldsymbol{q})$ is obtained from

$$\boldsymbol{R}(\boldsymbol{q}) = (2q_o^2 - 1)\mathbf{1}_3 + 2q_o\lceil \boldsymbol{q}_v \rceil + 2\boldsymbol{q}_v\boldsymbol{q}_v^T \tag{28}$$

As seen from Eqs. (26) and (27), the sensor outputs are nonlinear functions of the quaternions $\boldsymbol{q}$ and $\boldsymbol{\eta}$, which are not among the system states; rather, the state vector contains the quaternion variations $\delta\boldsymbol{q}_v$ and $\delta\boldsymbol{\eta}_v$ instead. Therefore, to implement the state estimator, we need to write the observation vector $\boldsymbol{z}_k$ in terms of the noisy position measurements of the camera, $\breve{\boldsymbol{r}}_{c_k}$, and the orientation $\breve{\boldsymbol{\mu}}_k$ as

$$\boldsymbol{z}_k = \boldsymbol{h}(\breve{\boldsymbol{r}}_{c_k}, \breve{\boldsymbol{\mu}}_k) \triangleq \begin{bmatrix} \breve{\boldsymbol{r}}_{c_k} - \boldsymbol{\rho}_c \\ \mathrm{vec}(\bar{\boldsymbol{\eta}}_k^* \otimes \breve{\boldsymbol{\mu}}_k \otimes \bar{\boldsymbol{q}}_k^*) \end{bmatrix} \tag{29}$$

which will be used in the innovation step of the Kalman filter [see Eq. (46b)]. On the other hand, using relations (7), (18), (26), and (27) in Eq. (29), we can rewrite the preceding equation as a function of states χ_k as

$$\boldsymbol{z}_k = \boldsymbol{h}_k(\boldsymbol{\chi}_k) + \boldsymbol{v}_k \tag{30}$$

where

$$\boldsymbol{h}_k(\boldsymbol{\chi}_k) = \begin{bmatrix} \boldsymbol{r}_k + \boldsymbol{R}(\boldsymbol{q}_k)\boldsymbol{\rho}_{t_k} \\ \mathrm{vec}(\delta\boldsymbol{\eta}_k \otimes \delta\boldsymbol{q}_k) \end{bmatrix}$$

with $\boldsymbol{z}_k^T = [\,\boldsymbol{z}_{1_k}^T \quad \boldsymbol{z}_{2_k}^T\,]$, $\boldsymbol{h}_k^T = [\,\boldsymbol{h}_{1_k}^T \quad \boldsymbol{h}_{2_k}^T\,]$, and $\boldsymbol{v}_k^T = [\,\boldsymbol{v}_{1_k}^T \quad \boldsymbol{v}_{2_k}^T\,]$, where $\boldsymbol{v}_{1_k}$ and $\boldsymbol{v}_{2_k}$ are additive measurement-noise processes. Note that the discrete-time observation vector (30) is now a nonlinear function of the states. To linearize the observation vector, one also needs to derive the sensitivity of the nonlinear observation vector with respect to the system states. Because $\boldsymbol{q} = \delta\boldsymbol{q} \otimes \bar{\boldsymbol{q}}$, we will have

$$\boldsymbol{h}_{1_k} = \boldsymbol{r}_k + \boldsymbol{R}(\delta\boldsymbol{q}_k \otimes \bar{\boldsymbol{q}}_k)\boldsymbol{\rho}_{t_k} \tag{31}$$

thus resulting in

$$\frac{\partial \boldsymbol{h}_{1_k}}{\partial \boldsymbol{\rho}_{t_k}} = \boldsymbol{R}(\delta\boldsymbol{q}_k \otimes \bar{\boldsymbol{q}}_k) = \boldsymbol{R}(\bar{\boldsymbol{q}}_k)\boldsymbol{R}(\delta\boldsymbol{q}_k) \tag{32}$$

On the other hand, it can readily be seen from Eq. (28) that for a small rotation $\delta\boldsymbol{q}$ (i.e., $\|\delta\boldsymbol{q}_v\| \ll 1$ and $\delta q_0 \approx 1$), we have

$$\boldsymbol{R}(\delta\boldsymbol{q}) \approx \mathbf{1}_3 + 2\lceil \delta\boldsymbol{q}_v \rceil$$

Hence, Eq. (31) can be approximated as

$$\boldsymbol{h}_{1_k} \approx \boldsymbol{r}_k + \boldsymbol{R}(\bar{\boldsymbol{q}}_k)(\mathbf{1}_3 + 2\lceil \delta\boldsymbol{q}_{v_k} \rceil)\boldsymbol{\rho}_{t_k}$$

in which we have used the identity $\boldsymbol{R}(\boldsymbol{q}_1 \otimes \boldsymbol{q}_2) \equiv \boldsymbol{R}(\boldsymbol{q}_2)\boldsymbol{R}(q_1)$. Thus, in view of the identity $\lceil \boldsymbol{a} \rceil \boldsymbol{b} \equiv -\lceil \boldsymbol{b} \rceil \boldsymbol{a}$, we can readily obtain

$$\frac{\partial \boldsymbol{h}_{1_k}}{\partial \delta\boldsymbol{q}_{v_k}} = -2\boldsymbol{R}(\bar{\boldsymbol{q}}_k)\lceil \boldsymbol{\rho}_{t_k} \rceil \tag{33}$$

Moreover, from Eqs. (2) and (30), we have

$$\boldsymbol{h}_{2_k} = \mathrm{vec}(\delta\boldsymbol{\eta}_k \otimes \delta\boldsymbol{q}_k) = \mathrm{vec}(\delta\boldsymbol{q}_k \circledast \delta\boldsymbol{\eta}_k) \tag{34}$$

which is a bilinear function of the state variables. Therefore, the following partial derivatives are derived from Eq. (34) as

$$\frac{\partial \boldsymbol{h}_{2_k}}{\partial \delta\boldsymbol{q}_{v_k}} = -\lceil \delta\boldsymbol{\eta}_{v_k} \rceil + \delta\eta_{o_k}\mathbf{1}_3 - \delta q_{o_k}^{-1}\delta\boldsymbol{\eta}_{v_k}\delta\boldsymbol{q}_{v_k}^T \tag{35}$$

$$\frac{\partial \boldsymbol{h}_{2_k}}{\partial \delta\boldsymbol{\eta}_{v_k}} = \lceil \delta\boldsymbol{q}_{v_k} \rceil + \delta q_{o_k}\mathbf{1}_3 - \delta\eta_{o_k}^{-1}\delta\boldsymbol{q}_{v_k}\delta\boldsymbol{\eta}_{v_k}^T \tag{36}$$

Neglecting the second-order term $\delta\boldsymbol{\eta}_{v_k}\delta\boldsymbol{q}_{v_k}^T$, in view of Eqs. (32), (33), (35), and (36), we can write the sensitivity matrix as

$$\boldsymbol{H}_k = \begin{bmatrix} -2\boldsymbol{R}(\bar{\boldsymbol{q}}_k)\lceil \rho_{t_k} \rceil & \mathbf{0}_{3\times6} & \mathbf{1}_3 & \mathbf{0}_{3\times3} & \boldsymbol{R}(\bar{\boldsymbol{q}}_k) & \mathbf{0}_{3\times3} \\ -\lceil \delta\boldsymbol{\eta}_{v_k} \rceil + \delta\eta_{o_k}\mathbf{1}_3 & \mathbf{0}_{3\times6} & \mathbf{0}_{3\times3} & \mathbf{0}_{3\times3} & \mathbf{0}_{3\times3} & \lceil \delta\boldsymbol{q}_{v_k} \rceil + \delta q_{o_k}\mathbf{1}_3 \end{bmatrix}$$

where $\delta\boldsymbol{\eta}_v$ is assumed to be sufficiently small so that $\delta\eta_{o_k}$ can unambiguously be obtained as $\delta\eta_{o_k} = (1 - \|\delta\boldsymbol{\eta}_{v_k}\|^2)^{1/2}$. Therefore, the linearized measurement equation is obtained as

$$\boldsymbol{z}_k = \boldsymbol{H}_k\boldsymbol{\chi}_k + \boldsymbol{v}_k$$

D. Propagation of Measurement Noise

The KF requires knowledge of the covariance matrix of the measurement noise. The challenge in modeling the quaternion error in the form of additive noise is that the unit-norm property of the quaternion must be preserved. That imposes a constraint on the additive noise, thus leading to a state-dependent covariance matrix, as seen in Sec. III.D.1. On the other hand, if the vision system gives the target orientation in form of the Euler angles, which are then transformed into quaternion representation, Euler-angle errors are propagated to the corresponding observation error through a transformation matrix derived in Sec. III.D.2.

1. Noise Characteristic Pertaining to Quaternion Normalization

When an additive quaternion noise process $\boldsymbol{\epsilon}_\mu$ is added to the quaternion measurement, the quaternion has to be normalized. Denoting the normalized quaternion with $\boldsymbol{\epsilon}_\mu$, we have

$$\breve{\boldsymbol{\mu}} = \breve{\boldsymbol{\mu}}(\boldsymbol{\mu}, \boldsymbol{\epsilon}_\mu) = \frac{\boldsymbol{\mu} + \boldsymbol{\epsilon}_\mu}{\|\boldsymbol{\mu} + \boldsymbol{\epsilon}_\mu\|} \tag{37}$$

$$\approx \boldsymbol{\mu} + (1_4 - \boldsymbol{\mu}\boldsymbol{\mu}^T)\boldsymbol{\epsilon}_\mu \tag{38}$$

where approximation Eq. (38) is derived by expanding Taylor's series for Eq. (37) about $\boldsymbol{\epsilon}_\mu = \mathbf{0}_{4\times1}$. Thus, we will have

$$\begin{aligned} z_2 = \mathrm{vec}(\bar{\boldsymbol{\eta}}^* \otimes \breve{\boldsymbol{\mu}}(\boldsymbol{\mu}, \boldsymbol{\epsilon}_\mu) \otimes \bar{\boldsymbol{q}}^*) &\approx \boldsymbol{h}_2 + \mathrm{vec}(\bar{\boldsymbol{\eta}}^* \otimes \boldsymbol{\epsilon}_\mu \otimes \bar{\boldsymbol{q}}^*) \\ &- \mathrm{vec}(\bar{\boldsymbol{\eta}}^* \otimes (\bar{\boldsymbol{\mu}}\bar{\boldsymbol{\mu}}^T\boldsymbol{\epsilon}_\mu) \otimes \bar{\boldsymbol{q}}^*) \end{aligned} \tag{39}$$

Using the properties of quaternion kinematics and that [by definition, Eq. (26)] $\bar{\boldsymbol{\mu}} = \bar{\boldsymbol{\eta}} \otimes \bar{\boldsymbol{q}}$, we obtain

$$\bar{\boldsymbol{\eta}}^* \otimes (\bar{\boldsymbol{\mu}}\bar{\boldsymbol{\mu}}^T\boldsymbol{\epsilon}_\mu) \otimes \bar{\boldsymbol{q}}^* = \begin{bmatrix} \mathbf{0}_{3\times1} \\ \bar{\boldsymbol{\mu}}^T\boldsymbol{\epsilon}_\mu \end{bmatrix}$$

The preceding identity implies that the last term on the RHS of Eq. (39) is zero. Therefore, it is the second term on the RHS of Eq. (39) that accounts for the attitude measurement noise; that is,

$$\boldsymbol{v}_{2_k} = \boldsymbol{T}_{\mu_k}\boldsymbol{\epsilon}_{\mu_k}$$

where

$$\boldsymbol{T}_{\mu_k} \triangleq [\,\mathbf{1}_3 \quad \mathbf{0}_{3\times1}\,]\bar{\boldsymbol{\eta}}_k^* \otimes \bar{\boldsymbol{q}}_k^* \circledast$$

One can then relate the covariance matrices through

$$\boldsymbol{S}_k \triangleq E[\boldsymbol{v}_k\boldsymbol{v}_k^T] = \mathrm{diag}(\boldsymbol{\Sigma}_r, \boldsymbol{T}_{\mu_k}\boldsymbol{\Sigma}_{\mu_k}\boldsymbol{T}_{\mu_k}^T) \tag{40}$$

2. Noise Characteristic Pertaining to Euler-Angle-to-Quaternion Transformation

Only three elements of the quaternion are independent. Thus, it appears appropriate to use a three-variable representation of orientation to model the source of the orientation noise. From the many possibilities, we choose the pitch-roll-yaw representation with regard to the LCS frame and represent the angles by $\boldsymbol{\varphi}^T \triangleq [\,\alpha \quad \beta \quad \gamma\,]$.

Because quaternion $\boldsymbol{\mu}$ is a nonlinear function of the independent variable $\boldsymbol{\varphi}$ [i.e., $\boldsymbol{\mu} = \boldsymbol{\mu}(\boldsymbol{\varphi})$], any error in the Euler angles propagates nonlinearly to the corresponding quaternion. However, by linearizing $\boldsymbol{\mu}(\boldsymbol{\varphi})$, we obtain

$$\breve{\boldsymbol{\mu}} = \breve{\boldsymbol{\mu}}(\bar{\boldsymbol{\varphi}} + \boldsymbol{\epsilon}_\varphi) \approx \boldsymbol{\mu}(\bar{\boldsymbol{\varphi}}) + \left(\frac{\partial \boldsymbol{\mu}}{\partial \boldsymbol{\varphi}}\right)_{\boldsymbol{\varphi}=\bar{\boldsymbol{\varphi}}} \boldsymbol{\epsilon}_\varphi \tag{41}$$

which allows the linear propagation of the independent white noise $\boldsymbol{\epsilon}_\varphi$ to the quaternion. To obtain the Jacobian in Eq. (41), we note that the angular velocity $\boldsymbol{\omega}_\mu$ associated with the orientation $\boldsymbol{\mu}$ is related to the time derivative of the corresponding Euler angles through

$$\boldsymbol{\omega}_\mu = \boldsymbol{C}\dot{\boldsymbol{\varphi}} \tag{42}$$

where

$$\boldsymbol{C} \triangleq \begin{bmatrix} -\sin\beta & 0 & 1 \\ \cos\beta\sin\gamma & \cos\gamma & 0 \\ \cos\beta\cos\gamma & -\sin\gamma & 0 \end{bmatrix}$$

On the other hand, from $\dot{\boldsymbol{\mu}} = \frac{1}{2}\boldsymbol{\mu} \circledast \underline{\boldsymbol{\omega}}_\mu$ and $\partial\boldsymbol{\mu}/\partial\boldsymbol{\varphi} \equiv \partial\dot{\boldsymbol{\mu}}/\partial\dot{\boldsymbol{\varphi}}$, one can arrive at

$$\frac{\partial \boldsymbol{\mu}}{\partial \boldsymbol{\varphi}} = \frac{1}{2}[\boldsymbol{\mu}\circledast]\begin{bmatrix} \boldsymbol{C} \\ \boldsymbol{0}_{1\times 3} \end{bmatrix}$$

which can be substituted in Eq. (41) to get

$$\breve{\boldsymbol{\mu}}(\bar{\boldsymbol{\varphi}} + \boldsymbol{\epsilon}_\varphi) \approx \boldsymbol{\mu}(\bar{\boldsymbol{\varphi}}) + \frac{1}{2}\bar{\boldsymbol{\mu}} \circledast \begin{bmatrix} \boldsymbol{C}\boldsymbol{\epsilon}_\varphi \\ \boldsymbol{0} \end{bmatrix}$$

In view of Eq. (2) and that $\bar{\boldsymbol{\mu}} = \bar{\boldsymbol{\eta}} \otimes \bar{\boldsymbol{q}}$, we can find the propagation of Euler-angle error $\boldsymbol{\epsilon}_\varphi$ to the corresponding observation error $\boldsymbol{v}_{2_k}$ in a development similar to Eq. (37); that is,

$$\begin{aligned} \boldsymbol{v}_2 &= \frac{1}{2}\mathrm{vec}\left(\bar{\boldsymbol{\eta}}^* \otimes \left(\begin{bmatrix} \boldsymbol{C}\boldsymbol{\epsilon}_\varphi \\ \boldsymbol{0}_{1\times 3} \end{bmatrix} \otimes (\bar{\boldsymbol{\eta}} \otimes \bar{\boldsymbol{q}})\right) \otimes \bar{\boldsymbol{q}}^*\right) \\ &= \frac{1}{2}\mathrm{vec}\left([\bar{\boldsymbol{\eta}}^*\otimes][\bar{\boldsymbol{\eta}}\circledast]\begin{bmatrix} \boldsymbol{C}\boldsymbol{\epsilon}_\varphi \\ \boldsymbol{0}_{1\times 3} \end{bmatrix}\right) \end{aligned}$$

It is known that any quaternion $\boldsymbol{a}$ satisfies the following useful identity [21]:

$$[\boldsymbol{a}\otimes][\boldsymbol{a}^*\circledast] = \begin{bmatrix} \boldsymbol{R}(\boldsymbol{a}) & \boldsymbol{0}_{3\times 1} \\ \boldsymbol{0}_{1\times 3} & 1 \end{bmatrix}$$

which can be used to simplify the noise expression as

$$\boldsymbol{v}_{2_k} = \boldsymbol{T}_{\varphi_k}\boldsymbol{\epsilon}_{\varphi_k}$$

where

$$\boldsymbol{T}_{\varphi k} \triangleq \tfrac{1}{2}\boldsymbol{R}^T(\bar{\boldsymbol{\eta}}_k)\boldsymbol{C}$$

The covariance matrix of the observation noise can then be obtained in the same way as Eq. (40).

IV. Filter Design

Let us compose the continuous-time states of the system as

$${}^a\boldsymbol{\chi} = [\,\boldsymbol{q}^T \quad \boldsymbol{\omega}^T \quad \boldsymbol{p}^T \quad \boldsymbol{r}^T \quad \dot{\boldsymbol{r}}^T \quad \boldsymbol{\rho}_t^T \quad \boldsymbol{\eta}^T\,]^T \in \mathbb{R}^{23} \tag{43}$$

It should be noted that the difference between ${}^a\boldsymbol{\chi}$ and $\boldsymbol{\chi}$, as defined in Eqs. (17) and (43), is that the former contains the full quaternions $\boldsymbol{q}$ and $\boldsymbol{\eta}$ and the latter includes the vector parts of their variations, $\delta\boldsymbol{q}_v$ and $\delta\boldsymbol{\eta}_v$. Combining Eqs. (6), (9), (14), and (13) and $\dot{\boldsymbol{p}} = 0$, we then obtain the state-space model of the system as

$${}^a\dot{\boldsymbol{\chi}} = \boldsymbol{f}({}^a\boldsymbol{\chi}, \boldsymbol{\epsilon}) \tag{44}$$

where $\boldsymbol{\epsilon} = [\,\boldsymbol{\epsilon}_\tau^T \quad \boldsymbol{\epsilon}_f^T\,]^T$. The quaternion variations can be obtained from the quaternions if the nominal value of the quaternions (i.e., $\bar{\boldsymbol{q}}_k$ and $\bar{\boldsymbol{\eta}}_k$) is given [see Eqs. (7) and (18)]. Because $\boldsymbol{\eta}_k$ is constant, its nominal value is selected as $\bar{\boldsymbol{\eta}}_k = \hat{\boldsymbol{\eta}}_{k-1}$: namely, its last estimated value. The computation of $\bar{\boldsymbol{q}}_k$ is slightly more complicated due to the time-varying nominal angular velocity $\bar{\boldsymbol{\omega}}_{k-1} = \hat{\boldsymbol{\omega}}_{k-1}$. Defining the nominal trajectory of $\boldsymbol{q}$ as one governed by Eq. (6), with the initial condition $\bar{\boldsymbol{q}}_{k-1} = \hat{\boldsymbol{q}}_{k-1}$, we can compute $\bar{\boldsymbol{q}}_k$ from

$$\bar{\boldsymbol{q}}_k = e^{\frac{1}{2}T_\Delta[\underline{\hat{\boldsymbol{\omega}}}_{k-1}\otimes - \underline{\boldsymbol{n}}\circledast]}\hat{\boldsymbol{q}}_{k-1} \tag{d45}$$

where $\bar{\boldsymbol{\omega}}_{k-1}$ is considered to be constant. The preceding matrix exponential can, in general, be obtained as explained in Appendix C. If n is much smaller than ϖ_{k-1}, however, the matrix exponential in the preceding equation can be approximated as

$$\begin{aligned} e^{\frac{1}{2}T_\Delta[\underline{\hat{\boldsymbol{\omega}}}_{k-1}\otimes]} &= \left(\cos\frac{\varpi_{k-1}T_\Delta}{2} + \sin\frac{\varpi_{k-1}T_\Delta}{2}\right)\boldsymbol{1}_4 \\ &\quad - \frac{\varpi_{k-1}T_\Delta\cos(\varpi_{k-1}T_\Delta/2) - 4\sin(\varpi_{k-1}T_\Delta/2)}{2\varpi_{k-1}}[\underline{\hat{\boldsymbol{\omega}}}_{k-1}\otimes] \end{aligned}$$

The EKF-based observer for the associated noisy discrete system (19) is given in two steps:

Estimate correction:

$$\boldsymbol{K}_k = \boldsymbol{P}_k^- \boldsymbol{H}_k^T(\boldsymbol{H}_k\boldsymbol{P}_k^-\boldsymbol{H}_k^T + \boldsymbol{S}_k)^{-1} \tag{46a}$$

$$\hat{\boldsymbol{\chi}}_k = \hat{\boldsymbol{\chi}}_k^- + \boldsymbol{K}_k(\boldsymbol{z}_k - \boldsymbol{h}(\hat{\boldsymbol{\chi}}_k^-)) \quad \overset{(48)}{\rightarrow} \quad {}^a\hat{\boldsymbol{\chi}}_k \tag{46b}$$

$$\boldsymbol{P}_k = (\boldsymbol{1}_{21} - \boldsymbol{K}_k\boldsymbol{H}_k)\boldsymbol{P}_k^- \tag{46c}$$

Estimate propagation:

$${}^a\hat{\boldsymbol{\chi}}_{k+1}^- = {}^a\hat{\boldsymbol{\chi}}_k + \int_{t_k}^{t_{k+1}} \boldsymbol{f}({}^a\boldsymbol{\chi}(t), 0)\mathrm{d}t \tag{47a}$$

$$\boldsymbol{P}_{k+1}^- = \boldsymbol{\Phi}_k\boldsymbol{P}_k\boldsymbol{\Phi}_k^T + \boldsymbol{Q}_k \tag{47b}$$

Right after the innovation step (46b), the estimated quaternions $\hat{\boldsymbol{q}}_k$ and $\hat{\boldsymbol{\eta}}_k$ are computed from the estimated variations (namely, $\delta\hat{\boldsymbol{q}}_k$ and $\delta\hat{\boldsymbol{\eta}}_k$) as

$$\hat{\boldsymbol{q}}_k = \delta\hat{\boldsymbol{q}}_k \otimes \bar{\boldsymbol{q}}_k = \begin{bmatrix} \delta\hat{\boldsymbol{q}}_{v_k} \\ (1 - \|\delta\hat{\boldsymbol{q}}_{v_k}\|^2)^{\frac{1}{2}} \end{bmatrix} \otimes e^{\frac{1}{2}T_\Delta[\underline{\hat{\boldsymbol{\omega}}}_{k-1}\otimes - \underline{\boldsymbol{n}}\circledast]}\hat{\boldsymbol{q}}_{k-1} \tag{48a}$$

$$\hat{\boldsymbol{\eta}}_k = \delta\hat{\boldsymbol{\eta}}_k \circledast \bar{\boldsymbol{\eta}}_k = \begin{bmatrix} \delta\hat{\boldsymbol{\eta}}_{v_k} \\ (1 - \|\delta\hat{\boldsymbol{\eta}}_{v_k}\|^2)^{\frac{1}{2}} \end{bmatrix} \circledast \hat{\boldsymbol{\eta}}_{k-1} \tag{48b}$$

In summary, the state update at the innovation stage of the KF [namely, Eq. (46b)], may proceed through the following steps:

1) Vectors $\boldsymbol{z}_k$ and $\boldsymbol{h}_k(\hat{\boldsymbol{\chi}}_k^-)$ are obtained from Eqs. (29) and (30), respectively, based on the latest state estimate and pose measurement.

2) The reduced state vector $\hat{\boldsymbol{\chi}}_k$ is updated using Eq. (46b).

3) The quaternion estimates $\hat{\boldsymbol{q}}_k$ and $\hat{\boldsymbol{\eta}}_k$ are calculated from their estimated variations $\delta\hat{\boldsymbol{q}}_{v_k}$ and $\delta\hat{\boldsymbol{\eta}}_{v_k}$ using Eq. (48).

A. Noise-Adaptive Filter

In a noise-adaptive Kalman filter, the issue is that in addition to the states, the covariance matrix $\boldsymbol{S}_k$ of the measurement noise $\boldsymbol{v}_k$ has to be estimated. Starting with a batch-processing approach [25–27], we develop a recursive one to estimate the covariance matrix.

To that end, let us define

$$\boldsymbol{e}_k \triangleq \boldsymbol{z}_k - \boldsymbol{H}_k\hat{\boldsymbol{\chi}}_k^- \boldsymbol{H}_k(\hat{\boldsymbol{\chi}}_k - \hat{\boldsymbol{\chi}}_k^-) + \boldsymbol{v}_k$$

which, in fact, is a zero-mean white-noise sequence. Taking the covariances of both sides of the preceding equation yields

$$\boldsymbol{W}_k \triangleq E[\boldsymbol{e}_k \quad \boldsymbol{e}_k^T] = \boldsymbol{H}_k\boldsymbol{P}_k^-\boldsymbol{H}_k^T + \boldsymbol{S}_k$$

Therefore, an estimate of $\boldsymbol{S}_k$ can be obtained from

$$\hat{\boldsymbol{S}}_k = \hat{\boldsymbol{W}}_k - \boldsymbol{H}_k\boldsymbol{P}_k^-\boldsymbol{H}_k^T$$

where

$$\hat{\boldsymbol{W}}_k = \frac{1}{k}\sum_{i=1}^{k}\tilde{\boldsymbol{e}}_i\tilde{\boldsymbol{e}}_i^T, \quad \text{with} \quad \tilde{\boldsymbol{e}}_i = \boldsymbol{e}_i - \bar{\boldsymbol{e}}_i \tag{49}$$

where

$$\bar{\boldsymbol{e}}_i = \frac{1}{i}\sum_{j=1}^{i}\boldsymbol{e}_j$$

is the statistical sample mean. It can be shown that the batch processing (49) is equivalent to this recursive formulation:

$$\tilde{\boldsymbol{e}}_k = \frac{k-1}{k}\tilde{\boldsymbol{e}}_{k-1} + \frac{k-1}{k}(\boldsymbol{e}_k - \boldsymbol{e}_{k-1}) \tag{50a}$$

$$\hat{\boldsymbol{W}}_k = \frac{k-1}{k}\hat{\boldsymbol{W}}_{k-1} + \frac{1}{k}\tilde{\boldsymbol{e}}_k\tilde{\boldsymbol{e}}_k^T \tag{50b}$$

Clearly, the dynamics equation (50b) preserves the positive definiteness of $\hat{\boldsymbol{W}}_k$ if it is appropriately initialized. Thereafter, $\hat{\boldsymbol{W}}_k^{-1}$, required for Eq. (46a), remains well defined for all k.

B. Predictor

Having estimated the full states and the parameters at a given point in time, one can integrate the dynamics model ${}^a\dot{\boldsymbol{\chi}} = \boldsymbol{f}({}^a\hat{\boldsymbol{\chi}}, \boldsymbol{0})$ to predict the ensuing motion of the target satellite from that point on [9]. Despite ignoring the effects of the force and the torque perturbations $\boldsymbol{\epsilon}$ in the dynamics equation, the trajectories can still be obtained within a reasonable accuracy from the estimates of the states and the system parameters. The reason is that the perturbations are small in magnitude.

The range data from the LCS along with the CAD model of the target satellite are used by a modified version of the iterative closest point (ICP) algorithm [28,29] to estimate the target pose. The ICP basically is a search algorithm that tries to find the best possible match between the 3-D data of the LCS and a model within the neighborhood of the previous pose [9]. In other words, the LCS sequentially estimates the current pose based on the previous one, which makes the estimation process fragile. This is because if the ICP does not converge for a particular pose, in the next estimation step, the initial guess of the pose may be too far from its actual value. If the initial pose happens to be outside the convergence region of the ICP process, from that point on, the pose tracking is most likely lost for good. The predictor can be made more robust by placing the ICP and the adaptive predictor in a closed-loop configuration, whereby the initial guess for the ICP is provided by the predictor. Then the pose-tracking process becomes inherently robust because, even if the ICP does not converge, the predictor can still provide a reliable initial guess for the forthcoming ICP steps.

V. Simulation

The convergence properties of the adaptive KF were investigated through simulations. For our simulations, a Canadian microsatellite called QuickSat was selected as the target satellite, which has the following principal moments of inertia: $I_{xx} = 4\ \text{kg}\cdot\text{m}^2$, $I_{yy} = 8\ \text{kg}\cdot\text{m}^2$, and $I_{zz} = 5\ \text{kg}\cdot\text{m}^2$. The LCS observes the position of a point of reference located at

$$\boldsymbol{\rho}_t = [0.2 \quad 0.1 \quad 0.05]^T\ \text{m}$$

and the attitude of a frame for which the orientation with regard to the target principal axes is described by quaternion

$$\boldsymbol{\eta} = [0.12 \quad 0.05 \quad -0.15 \quad 0.98]^T$$

The target and the chaser satellites traverse in circular orbits at the rate $n = 0.0012$ rad/s. The vision system is affected by measurement-noise processes with covariances $\boldsymbol{\Sigma}_r = 3\times10^{-3}\boldsymbol{1}_3\ \text{m}^2$ and $\boldsymbol{\Sigma}_\mu = 5\times10^{-3}\boldsymbol{1}_4$, which are typical representations of the noise characteristics of an active vision system [29,30]. Note that in our simulation, the noise parameters are not known by the estimator; rather, our estimator begins with initial values that are far away from the true covariances (i.e., with considerable errors of 100%). The covariances of the process noise representing the orbital force/torque perturbations are set to $\boldsymbol{\Sigma}_f = 2\times10^{-6}\boldsymbol{1}_3\ \text{m}^2/\text{s}^4$ and $\boldsymbol{\Sigma}_\tau = 2.5\times10^{-5}\boldsymbol{1}_3\ \text{rad}^2/\text{s}^4$.

The trajectories of the measured, the estimated, and the actual poses are depicted in Figs. 2 and 3, which display the trajectories of the estimated as well as the actual angular velocities. As seen, after some period of time, the estimated values converge to the actual values. The angular and translational velocity estimates, however, are not as accurate as the pose estimates, because the filter does not receive any direct velocity measurements. The measured and the estimated pose errors are shown in Fig. 4, which illustrates how the

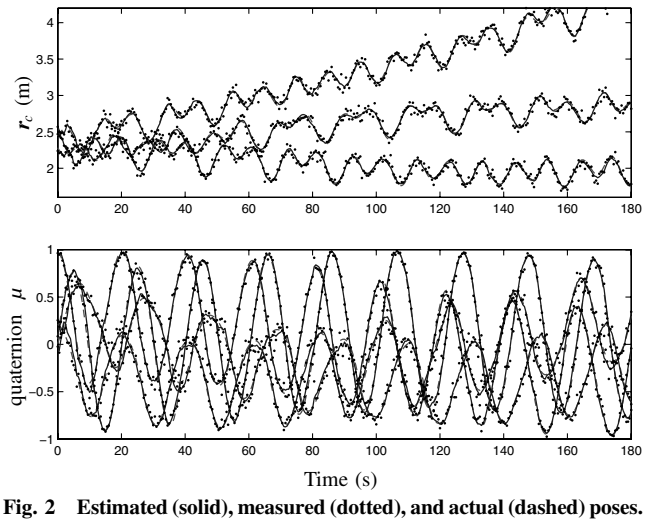

Fig. 2 Estimated (solid), measured (dotted), and actual (dashed) poses.

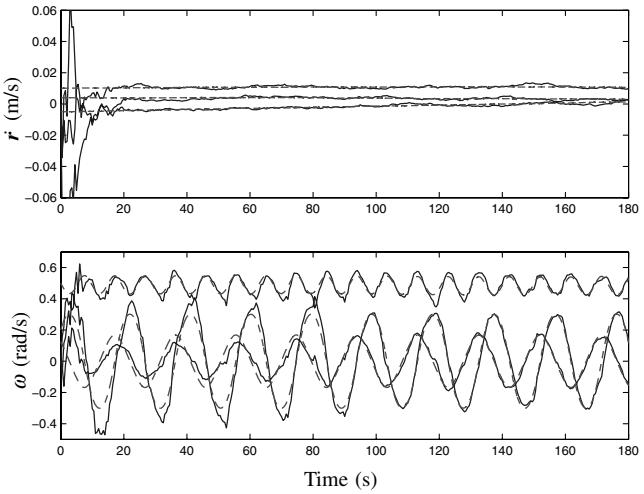

Fig. 3 Estimated (solid) and actual (dashed) translational and angular velocities.

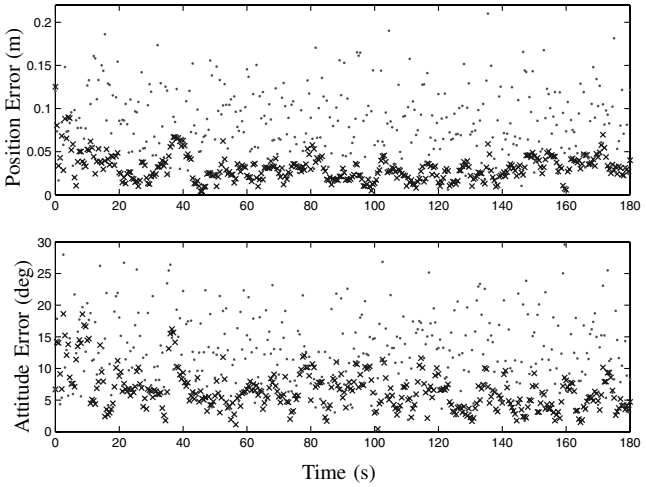

Fig. 4 Comparison between the position and orientation errors without (dot) and with (cross) Kalman filtering.

filter reduces the measurement error. Here, the errors are simply measured as follows.

Position error:

$$\|\hat{\boldsymbol{r}}_c - \boldsymbol{r}_c\|$$

Orientation error:

$$2\sin^{-1}\|\mathrm{vec}(\boldsymbol{\mu} \otimes \hat{\boldsymbol{\mu}}^*)\|$$

where $\hat{\boldsymbol{r}}_c$ and $\hat{\boldsymbol{\mu}}$ are the estimated distance and the quaternion, respectively. Finally, Figs. 5 and 6 illustrate the time history of the estimated parameters as well as the diagonal elements of the estimated covariance matrices of the noise processes associated with the pose measurement. The results clearly show that the parameter estimates very well converge to the actual values despite starting with large initial errors.

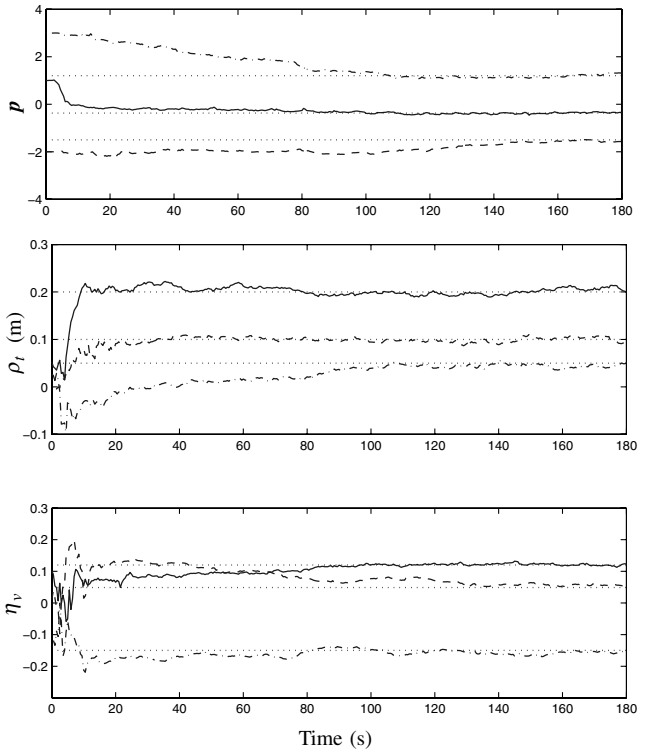

Fig. 5 Convergence of the estimated parameters to their true values.

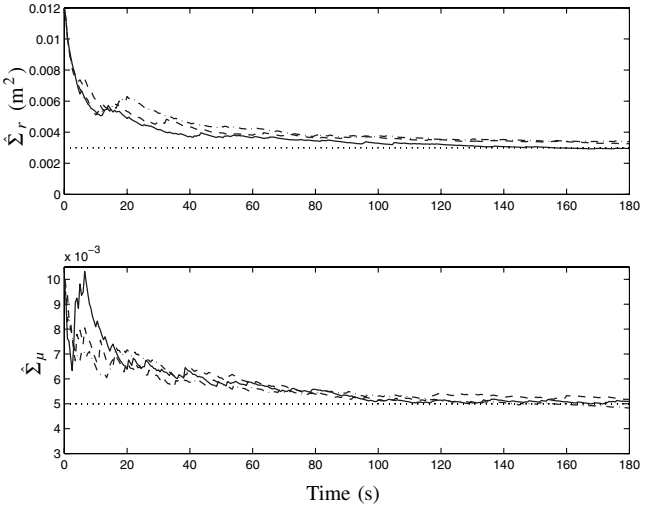

Fig. 6 Convergence of the estimated measurement-noise covariances.

VI. Experiment

Our main objective of experimentation was to demonstrate that the adaptive KF was real-time implementable. Another objective was to show that the filter could reliably and accurately provide pose information when vision data (due to occlusion, for instance) became unavailable. In such a case, the adaptive filter relies on the model as well as the past state and parameter estimates to produce the best possible estimates of the current pose. Therefore, the robotic capture of a tumbling satellite will become possible even if the vision system is fully occluded. In this experiment, we also demonstrated that an accurate long-term prediction of the motion trajectory of the target satellite was possible. This is critical for any trajectory planning approach whereby the robot is to intercept the target at a rendezvous point [10,12,13].

Shown in Fig. 7 is our experimental setup, which included a two-thirds mockup of QuickSat as the target satellite. The mockup was moved by a manipulator according to orbital dynamics. For the spacecraft simulator that drove the manipulator, parameters were

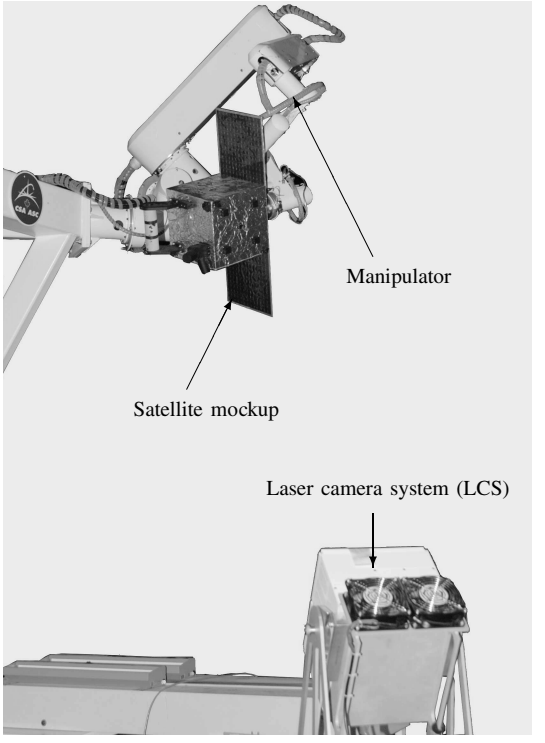

Fig. 7 Experimental setup.

selected as $I_{xx} = 4\ \text{kg} \cdot \text{m}^2$, $I_{yy} = 8\ \text{kg} \cdot \text{m}^2$, $I_{zz} = 5\ \text{kg} \cdot \text{m}^2$, and $\boldsymbol{\rho}_t^T = [-0.15 \quad 0 \quad 0]$ m, which represented the dynamics parameters of Quicksat. To be able to evaluate the accuracy of the estimated and the predicted poses, the actual pose was directly computed using the manipulator kinematics. The LCS was used to obtain the pose measurements at a rate of 2 Hz. Note that the predictor had no a priori knowledge of either the inertia properties of the target satellite or the noise properties of the vision sensor.

In the experiment, the field of view of the LCS was intentionally occluded at $t = 140$ s. From that moment on, the predictor relied solely on the values of the latest estimate of the states and parameters to predict the future trajectory. Figures 8–10, show the trajectories of the estimated velocities, parameters, and measurement covariances, respectively. The true values of the parameters are depicted by dotted lines in Fig. 9. It is evident from the graphs that the estimator converged after about 120 s. The trajectories of the predicted and the actual poses (obtained from the kinematics of the robot) are plotted in Fig. 11. The results show that the adaptive EKF continued to provide accurate pose estimates even after the vision system was occluded, and it consequently failed to provide any pose data past $t = 140$ s. This demonstrates the excellent performance of the EKF in providing reliable estimates of the pose of the target satellite in spite of the failure of the vision system.

During the experiments, the pose of the target was predicted 20 s into the future using the adaptive predictor. The prediction results are

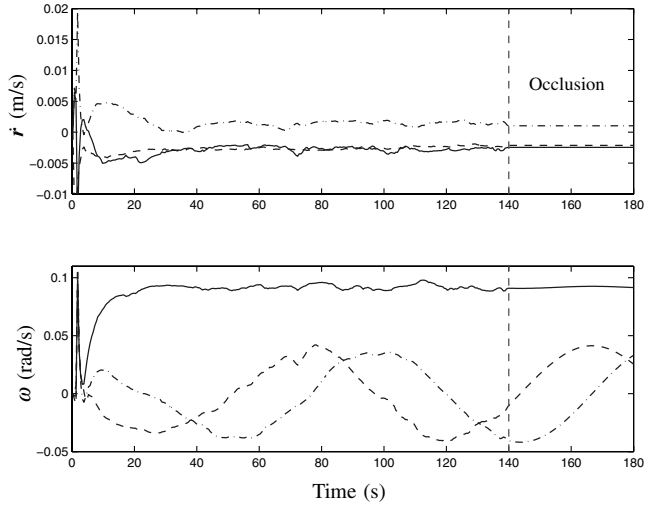

Fig. 8 Estimated translational and angular velocities.

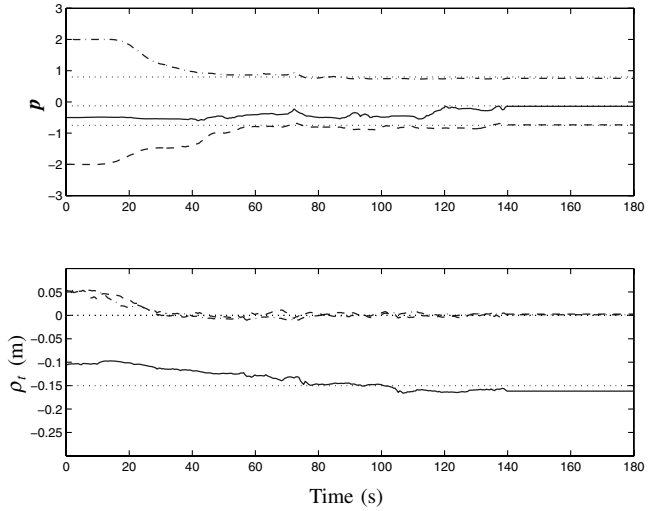

Fig. 9 Convergence of the estimated parameters to their true values (dotted lines).

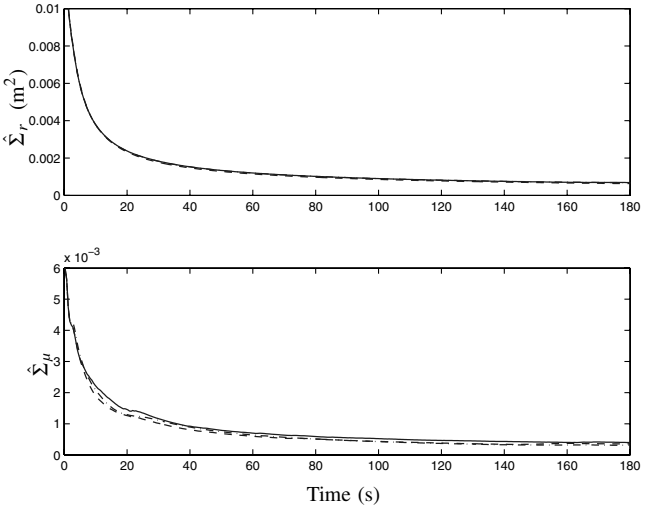

Fig. 10 Convergence of the estimated covariances of the measurement noise.

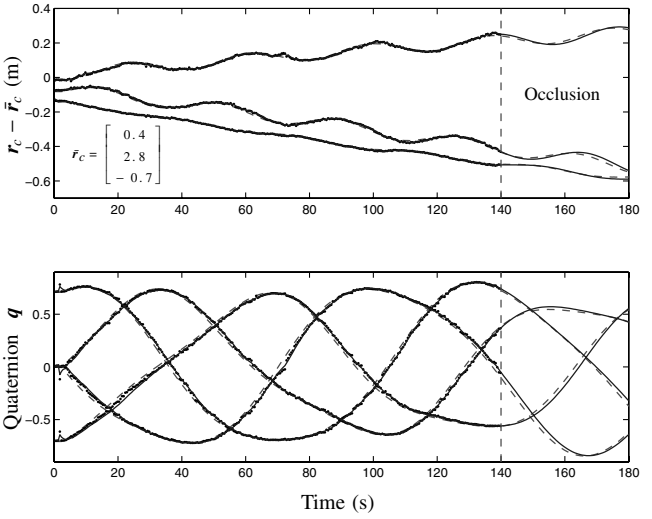

Fig. 11 Estimated (solid), actual (dashed), and measured (dotted) poses.

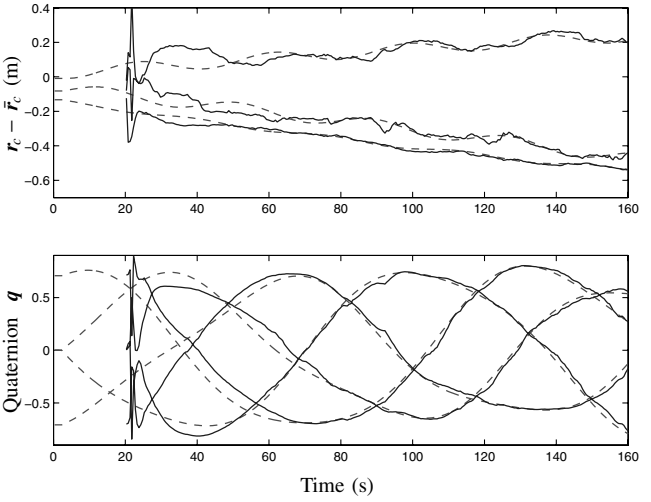

Fig. 12 Predicted (solid) and actual (dashed) poses.

given in Fig. 12 along with the actual pose, and the associated prediction error is plotted in Fig. 13. The figures show that after about 60 s of prediction, the predictor output was closely following the actual motion. Both attitude and position errors in predicted pose

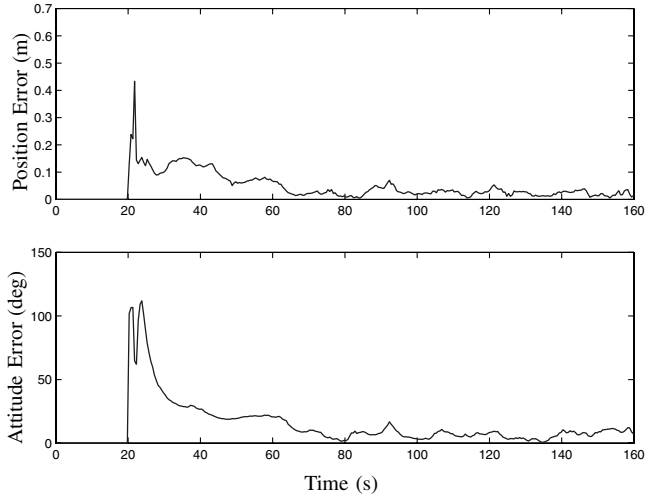

Fig. 13 Error incurred in the prediction of pose 20 s in advance.

became considerably small after 80 s. However, it appears that the predictor performed better with position. The reason may be that the rotational motion of the target was not rich enough, which is to be expected, because a tumbling satellite will be rotating mostly about its major principal axis.

VII. Conclusions

A computationally efficient adaptive Kalman filter was developed that used the noisy measurements provided by a laser-vision system to estimate and predict the relative position, orientation, and velocities (both translational and angular) of two free-falling satellites that move in close orbits near each other. In addition to the preceding kinematic variables, the adaptive filter produces all inertia parameters of the target satellite as well as the covariance of the measurement noise. A simple decoupled dynamics model was developed by writing the dynamics equations pertaining to the translational and rotational dynamics in the chaser and the target body-attached frames, respectively. Another feature of our model was that the majority of the unknown parameters appeared only in the observation equations and all the Jacobian matrices required for linearization were expressed in closed forms. Moreover, the parameters pertaining to the orientation of the principal axes do not appear in the dynamics equations; rather, they merely enter in the observation equations.

The special structure of the linearized model was employed to derive closed-form expressions for both the state-transition matrix and the covariance of the process noise. The use of these expressions led to a computationally efficient discrete-time model suitable for real-time implementation of the adaptive Kalman filter. The variations of the quaternions from their nominal values were selected to be among the states of the system, so that the quaternion estimates can be consistently corrected in the innovation step of the filter. Furthermore, the propagation of the quaternion noise to the measurement noise was modeled using transformation matrices.

Finally, the convergence of the adaptive Kalman filter was demonstrated by both numerical and experimental results using the vision data provided by a space-qualified laser-vision system. It was also demonstrated through experiments that the adaptive filter could provide accurate pose data even when the vision system was occluded for tens of seconds.

Appendix A: Linearized Attitude Kinematics

To derive Eqs. (8), we start by differentiating Eq. (7) with respect to time:

$$\frac{d}{dt}\delta\boldsymbol{q} = \dot{\boldsymbol{q}} \otimes \bar{\boldsymbol{q}}^* + \boldsymbol{q} \otimes \dot{\bar{\boldsymbol{q}}}^* \tag{A1}$$

In the preceding equation, $\dot{\boldsymbol{q}}$ and $\dot{\bar{\boldsymbol{q}}}^*$ have to be written in terms of the angular velocity and its estimate. The expression for the former is readily available: namely, Eq. (6). For the latter, however, an expression can be obtained by noticing that

$$\frac{d}{dt}(\bar{\boldsymbol{q}} \otimes \bar{\boldsymbol{q}}^*) = \dot{\bar{\boldsymbol{q}}} \otimes \bar{\boldsymbol{q}}^* + \bar{\boldsymbol{q}} \otimes \dot{\bar{\boldsymbol{q}}}^* = \boldsymbol{0} \Rightarrow \dot{\bar{\boldsymbol{q}}}^* = -\bar{\boldsymbol{q}}^* \otimes \dot{\bar{\boldsymbol{q}}} \otimes \bar{\boldsymbol{q}}^* \tag{A2}$$

where $\dot{\bar{\boldsymbol{q}}}$ can be obtained in terms of $\bar{\boldsymbol{\omega}}$ using a relation similar to Eq. (6). Replacing $\dot{\boldsymbol{q}}$ and $\dot{\bar{\boldsymbol{q}}}^*$ in Eq. (A1) with their expressions and using Eq. (2), we obtain

$$\begin{aligned}
\frac{d}{dt}\delta\boldsymbol{q} &= \left[\frac{1}{2}(\underline{\boldsymbol{\omega}} \otimes -\underline{\boldsymbol{n}}\circledast)\boldsymbol{q}\right] \otimes \bar{\boldsymbol{q}}^* \\
&\quad - \boldsymbol{q} \otimes \left\{\bar{\boldsymbol{q}}^* \otimes \left[\frac{1}{2}(\bar{\boldsymbol{\omega}} \otimes -\underline{\boldsymbol{n}}\circledast)\bar{\boldsymbol{q}}\right] \otimes \bar{\boldsymbol{q}}^*\right\} \\
&= \frac{1}{2}[\underline{\boldsymbol{\omega}} \otimes \boldsymbol{q} \otimes \bar{\boldsymbol{q}}^* - \boldsymbol{q} \otimes \underline{\boldsymbol{n}} \otimes \bar{\boldsymbol{q}}^* \\
&\quad - \boldsymbol{q} \otimes \bar{\boldsymbol{q}}^* \otimes (\bar{\boldsymbol{\omega}} \otimes \bar{\boldsymbol{q}} \otimes \bar{\boldsymbol{q}}^* - \bar{\boldsymbol{q}} \otimes \underline{\boldsymbol{n}} \otimes \bar{\boldsymbol{q}}^*)] \\
&= \frac{1}{2}(\underline{\boldsymbol{\omega}} \otimes \delta\boldsymbol{q} - \delta\boldsymbol{q} \otimes \underline{\bar{\boldsymbol{\omega}}}) = \frac{1}{2}(\underline{\boldsymbol{\omega}} \otimes -\underline{\bar{\boldsymbol{\omega}}}\circledast)\delta\boldsymbol{q}
\end{aligned} \tag{A3}$$

Using Eq. (1), one can see that the vector part of the preceding quaternion equation results in

$$\begin{aligned}
\frac{d}{dt}\delta\boldsymbol{q}_v &= -\frac{1}{2}(\lceil\boldsymbol{\omega}\rceil + \lceil\bar{\boldsymbol{\omega}}\rceil)\delta\boldsymbol{q}_v + \frac{1}{2}(\boldsymbol{\omega} - \bar{\boldsymbol{\omega}})\delta q_0 \\
&= -\bar{\boldsymbol{\omega}} \times \delta\boldsymbol{q}_v - \frac{1}{2}\delta\boldsymbol{\omega} \times \delta\boldsymbol{q}_v + \frac{1}{2}\delta\boldsymbol{\omega}\delta q_0
\end{aligned} \tag{A4}$$

which, upon linearization, turns into the first of Eqs. (8). The second equation can similarly be derived from the scalar part of Eq. (A3).

Appendix B: Rotational System

Assuming that the spacecraft is acted upon by three independent disturbance torques about its principal axes, we can write Euler's equations as

$$I_{xx}\dot{\omega}_x = (I_{yy} - I_{zz})\omega_y\omega_z + \tau_x, \qquad I_{yy}\dot{\omega}_y = (I_{zz} - I_{xx})\omega_z\omega_x + \tau_y,$$
$$I_{zz}\dot{\omega}_z = (I_{xx} - I_{yy})\omega_x\omega_y + \tau_z$$

Rewriting the preceding equations in terms of perturbation $\epsilon_\tau = [\tau_x/I_{xx}\ \tau_y/I_{xx}\ \tau_z/I_{xx}]^T$, we obtain

$$\dot{\omega}_x = p_x\omega_y\omega_z + \epsilon_{\tau_x}, \qquad \dot{\omega}_y = p_z\omega_z\omega_x + \frac{I_{xx}}{I_{yy}}\epsilon_{\tau_y}$$
$$\dot{\omega}_z = p_z\omega_x\omega_y + \frac{I_{xx}}{I_{zz}}\epsilon_{\tau_z}$$

Finally, Eq. (9) can be obtained from the preceding equations by making use of the following identities:

$$\frac{I_{xx}}{I_{yy}} = \frac{1 - p_y}{1 + p_x}, \qquad \frac{I_{xx}}{I_{zz}} = \frac{1 + p_z}{1 - p_x}$$

Appendix C: Caley–Hamilton Theorem for Computing the Exponential Matrix

As a consequence of the Caley–Hamilton theorem, any power of a 3×3 matrix $\boldsymbol{M}$ greater than 2 can be obtained from its lower powers. Moreover, its exponential can be computed from the second-degree polynomial:

$$e^{\boldsymbol{M}t} = m_0\boldsymbol{1}_3 + m_1\boldsymbol{M} + m_2\boldsymbol{M}^2$$

The exponential of the eigenvalues of the matrix must satisfy the same polynomial; that is,

$$e^{\lambda_i t} = m_0(t) + m_1(t)\lambda_i + m_2(t)\lambda_i^2 \quad \text{for } i = 1, 2, 3 \tag{C1}$$

Therefore, if the eigenvalues are distinct, the coefficients of the polynomial can be found by solving the following linear system:

$$\begin{bmatrix} 1 & \lambda_1 & \lambda_1^2 \\ 1 & \lambda_2 & \lambda_2^2 \\ 1 & \lambda_3 & \lambda_3^2 \end{bmatrix} \begin{bmatrix} m_0 \\ m_1 \\ m_2 \end{bmatrix} = \begin{bmatrix} e^{\lambda_1 t} \\ e^{\lambda_2 t} \\ e^{\lambda_3 t} \end{bmatrix} \tag{C2}$$

where λ_i are the distinct eigenvalues of M; that is,

$$m_{k-1}(t) = \sum_{j=1}^{3} \gamma_{kj} e^{\lambda_j t} \quad \text{for } k = 1, 2, 3$$

where γ_{kj} are the entries of the inverse of the matrix in Eq. (C2). The characteristic equation

$$\lambda^3 + (p_y p_z \omega_x^2 + p_x p_z \omega_y^2 + p_x p_y \omega_z^2)\lambda + 2 p_x p_y p_z \omega_x \omega_y \omega_z = 0$$

can be solved with little effort due to its simple form.

If the eigenvalues are repeated, the rows of the coefficient matrix will be modified such that the corresponding repeated equations of Eq. (C1) will be replaced by the partial derivatives of the equation with respect to the repeated eigenvalue.

Appendix D: Scalar Functions

The scalar functions $\phi'_{jk}(t)$ in polynomial (20b) are calculated from

$$\phi'_{j1}(t) = \lambda_j^{-1}(e^{\lambda_j t} - 1),$$

$$\phi'_{j2}(t) = (\lambda_j^2 \varpi_k + \varpi_k^3)^{-1}(\varpi_k \cos \varpi_k t + \lambda_j \sin \varpi_k t - e^{\lambda_j t} \varpi_k),$$

$$\phi'_{j3}(t) = \varpi_k^{-2}\lambda_j^{-1} + (\lambda_j^3 \varpi_k^2 + \lambda_j \varpi_k^4)^{-1}(\lambda_j^2 \cos \varpi_k t - \varpi_k \lambda_j \sin \varpi_k t + \varpi_k^2 e^{\lambda_j t})$$

Similarly, the scalar functions $\phi'_{kj}(t)$ in Eq. (20e) are

$$\phi_{1j}(t) = \lambda_j^{-2}(1 - e^{\lambda_j t}) - \lambda_j^{-1} t,$$

$$\phi_{2j}(t) = (\lambda_j^3 \varpi_k^2 + \lambda_j \varpi_k^4)^{-1}(\varpi_k \lambda_j \sin \varpi_k t + \lambda_j^2 \cos \varpi_k t + \varpi_k^2 e^{\lambda_j t} - \lambda_j^2 - \varpi_k^2),$$

$$\phi_{3j}(t) = \varpi_k^{-2}\lambda_j^{-2} + (\lambda_j^4 \varpi_k^3 + \lambda_j^2 \varpi_k^5)^{-1}(\lambda_j^3 \sin \varpi_k t - \varpi_k \lambda_j^2 \cos \varpi_k t - \varpi_k^3 e^{-\lambda_j t} - (\varpi_k^3 \lambda_j + \lambda_j^3 \varpi_k) t)$$

References

[1] Zimpfer, D., and Spehar, P., "STS-71 Shuttle/MIR GNC Mission Overview," *Advances in Astronautical Sciences*, American Astronautical Society, San Diego, CA, 1996, pp. 441–460.

[2] Visentin, G., and Brown, D. L., "Robotics for Geostationary Satellite Service," *Robotics and Autonomous Systems*, Vol. 23, 1998, pp. 45–51. doi:10.1016/S0921-8890(97)00057-2

[3] Oda, M., "Space Robot Experiments on NASDA's ETS-VII Satellite—Preliminary Overview of the Experiment Results," *IEEE 1999 International Conference on Robotics and Automation (ICRA '99)*, Inst. of Electrical and Electronics Engineers, Piscataway, NJ, 1999, pp. 1390–1395.

[4] Ueno, H., Dubowsky, S., Lee, C., Zhu, C., Ohkami, Y., Matsumoto, S., and Oda, M., "Space Robotic Mission Concepts for Capturing Stray Objects," *Journal of Space Technology and Science*, Vol. 18, No. 2, 2002, pp. 1–8.

[5] Bornschlegl, E., Hirzinger, G., Maurette, M., Mugunolo, R., and Visentin, G., "Space Robotics in Europe, a Compendium," *Proceedings of the 7th International Symposium on Artificial Intelligence, Robotics, and Automation in Space (i-SAIRAS 2003)*, May 2003.

[6] Yoshida, K., "Engineering Test Satellite VII Flight Experiment for Space Robot Dynamics and Control: Theories on Laboratory Test Beds Ten Years Ago, Now in Orbit," *International Journal of Robotics Research*, Vol. 22, No. 5, 2003, pp. 321–335. doi:10.1177/0278364903022005003

[7] Samson, C., English, C., Deslauriers, A., Christie, I., Blais, F., and Ferrie, F., "Neptec 3D Laser Camera System: From Space Mission STS-105 to Terrestrial Applications," *Canadian Aeronautics and Space Journal*, Vol. 50, No. 2, 2004, pp. 115–123.

[8] Lichter, M. D., and Dubowsky, S., "State, Shape, and Parameter Estimation of Space Object from Range Images," *IEEE International Conference on Robotics and Automation*, Inst. of Electrical and Electronics Engineers, Piscataway, NJ, Apr. 2004, pp. 2974–2979.

[9] Hillenbrand, U., and Lampariello, R., "Motion and Parameter Estimation of a Free-Floating Space Object from Range Data for Motion Prediction," *8th International Symposium on Artificial Intelligence, Robotics, and Automation in Space (i-SAIRAS 2005)*, Sept. 2005.

[10] Sharma, R., Herve, J. Y., and Cuka, P., "Dynamic Robot Manipulation Using Visual Tracking," *IEEE International Conference Robotics & Automation*, Inst. of Electrical and Electronics Engineers, Piscataway, NJ, May 1992, pp. 1844–1849.

[11] Chen, Y., and Watson, L. T., "Optimal Trajectory Planning for a Space Robot Docking with a Moving Target via Homotopy Algorithms," *Journal of Robotic Systems*, Vol. 12, No. 8, 1995, pp. 531–540. doi:10.1002/rob.4620120803

[12] Croft, E. A., Fenton, R. G., and Benhabib, B., "Optimal Rendezvous-Point Selection for Robotic Interception of Moving Objects," *IEEE Transactions on Systems, Man, and Cybernetics*, Vol. 28, No. 2, Apr. 1998, pp. 192–204. doi:10.1109/3477.662759

[13] Mehrandezh, M., Sela, N. M., Fenton, R. G., and Benhabib, B., "Robotic Interception of Moving Objects Using an Augmented Ideal Proportional Navigation Guidance Technique," *IEEE Transactions on Systems, Man, and Cybernetics*, Vol. 30, No. 3, May 2000, pp. 238–250. doi:10.1109/3468.844351

[14] Masutani, Y., Iwatsu, T., and Miyazaki, F., "Motion Estimation of Unknown Rigid Body Under No External Forces and Moments," *IEEE International Conference on Robotics & Automation*, Inst. of Electrical and Electronics Engineers, Piscataway, NJ, May 1994, pp. 1066–1072.

[15] Kim, S.-G., Crassidis, J. L., Cheng, Y., Fosbury, A. M., and Junkins, J., "Kalman Filtering for Relative Spacecraft Attitude and Position Estimation," *Journal of Guidance, Control, and Dynamics*, Vol. 30, No. 1, Feb. 2007, pp. 133–143. doi:10.2514/1.22377

[16] Thienel, J. K., and Sanner, R. M., "Hubble Space Telescope Angular Velocity Estimation During the Robotic Servicing Mission," *Journal of Guidance, Control, and Dynamics*, Vol. 30, No. 1, Feb. 2007, pp. 29–34. doi:10.2514/1.20591

[17] Aghili, F., and Parsa, K., "Adaptive Motion Estimation of a Tumbling Satellite Using Laser-Vision Data with Unknown Noise Characteristics," *IEEE International Conference on Intelligent Robots and Systems*, Inst. of Electrical and Electronics Engineers, Piscataway, NJ, pp. 839–846, Oct. 29–2 Nov. 2007.

[18] van Loan, C. F., "Computing Integrals Involving the Matrix Exponential," *IEEE Transactions on Automatic Control*, Vol. 23, No. 3, June 1978, pp. 396–404.

[19] Wilcox, J. C., "A New Algorithm for Strapped-Down Inertial Navigation," *IEEE Transactions on Aerospace and Electronic Systems*, Vol. 3, No. 5, Sept. 1967, pp. 796–802.

[20] Lefferts, E. J., Markley, F. L., and Shuster, M. D., "Kalman Filtering for Spacecraft Attitude Estimation," *Journal of Guidance, Control, and Dynamics*, Vol. 5, No. 5, Sept.–Oct. 1982, pp. 417–429. doi:10.2514/3.56190

[21] Pittelkau, M. E., "Kalman Filtering for Spacecraft System Alignment Calibration," *Journal of Guidance, Control, and Dynamics*, Vol. 24, No. 6, Nov. 2001, pp. 1187–1195. doi:10.2514/2.4834

[22] Kaplan, M. H., *Modern Spacecraft Dynamics and Control*, Wiley, Hoboken, NJ, 1976, pp. 57–60.

[23] Clohessy, W. H., and Wiltshire, R. S., "Terminal Guidance System for Satellite Rendezvous," *Journal of Aerospace Science and Technology*, Vol. 27, No. 9, 1960, pp. 653–658.

[24] Chui, C. K., and Chen, G., *Kalman Filtering with Real-Time Applications*, Springer, Berlin, 1998, pp. 113–115.

[25] Kailath, T., "An Innovations Approach to Least-Squares Estimation, Part 1: Linear Filtering in Adaptive White Noise," *IEEE Transactions on Automatic Control*, Vol. 13, No. 6, 1968, pp. 646–655. doi:10.1109/TAC.1968.1099025

[26] Mehra, R. K., "On the Identification of Variances and Adaptive Kalman Filtering," *IEEE Transactions on Automatic Control*, Vol. 15, No. 2, Apr. 1970, pp. 175–184. doi:10.1109/TAC.1970.1099422

[27] Maybeck, P. S., *Stochastic Models, Estimation, and Control*, Vol 2, Academic Press, New York, 1982.

[28] Ruel, S., English, C., Anctil, M., and Church, P., "Lasso: Real-Time Pose Estimation from 3D Data for Autonomous Satellite Servicing,"

Proceedings of the 8th International Symposium on Artificial Intelligence, Robotics, and Automation in Space (i-SAIRAS 2005), Sept. 2005.

[29] Shang, L., Jasiobedzki, P., and Greenspan, M., "Discrete Pose Space Estimation to Improve ICP-Based Tracking," *Fifth International Conference on 3-D Digital Imaging and Modeling (3DIM'05)*, IEEE Computer Society, Washington, D.C., June 2005, pp. 523–530.

[30] English, C., Deslauriers, A., and Christie, I., "The Complementary Nature of Triangulation and Ladar Technologies," *Proceedings of SPIE, the International Society for Optical Engineering*, Society of Photo-Optical Instrumentation Engineers, Bellingham, WA, Apr. 2005, pp. 29–41.